THE UNIVERSITY OF ARIZONA
University Libraries

UA CAMPUS REPOSITORY

Development of a Remote Pulse Oximeter

Item Type	text; Electronic Thesis
Authors	Sankman, Joseph; Bailey, Brian; Ebel, Brian; Galvin, Scott; Grantham, Jack; Little, Scott; Morey, Erica; Stemple, Christopher
Citation	Sankman, Joseph, Bailey, Brian, Ebel, Brian, Galvin, Scott, Grantham, Jack, Little, Scott, Morey, Erica, & Stemple, Christopher. (2010). Development of a Remote Pulse Oximeter (Bachelor's thesis, University of Arizona, Tucson, USA).
Publisher	The University of Arizona.
Rights	Copyright © is held by the author. Digital access to this material is made possible by the University Libraries, University of Arizona. Further transmission, reproduction or presentation (such as public display or performance) of protected items is prohibited except with permission of the author.
Download date	07/02/2023 00:29:14
Item License	http://rightsstatements.org/vocab/InC/1.0/
Link to Item	http://hdl.handle.net/10150/146648

APPLE 1004

DEVELOPMENT OF A

REMOTE PULSE OXIMETER

By

BRIAN BAILEY
BRIAN EBEL
SCOTT GALVIN
JACK GRANTHAM
SCOTT LITTLE
ERICA MOREY
JOSEPH SANKMAN
CHRISTOPHER STEMPLE

A Thesis Submitted to The Honors College

In Partial Fulfillment of the Bachelors degree

With Honors in

Electrical Engineering

THE UNIVERSITY OF ARIZONA

May 2 0 1 0

Approved by:

Alonso Minjarez
Department of Electrical Engineering

The University of Arizona Electronic Theses and Dissertations Reproduction and Distribution Rights Form

Name (Last, First, Middle) Sankman, Joseph, A	
Degree title (eg BA, BS, BSE, BSB, BFA): BS Engineering	
Honors area (eg Molecular and Cellular Biology, English, Studio Art): Electrical Engineering	
Date thesis submitted to Honors College: 5-5-10	
Title of Honors thesis: Development of Remote Pulse Oximeter	
:The University of Arizona Library Release	I hereby grant to the University of Arizona Library the nonexclusive worldwide right to reproduce and distribute my dissertation or thesis and abstract (herein, the "licensed materials"), in whole or in part, in any and all media of distribution and in any format in existence now or developed in the future. I represent and warrant to the University of Arizona that the licensed materials are my original work, that I am the sole owner of all rights in and to the licensed materials, and that none of the licensed materials infringe or violate the rights of others. I further represent that I have obtained all necessary rights to permit the University of Arizona Library to reproduce and distribute any nonpublic third party software necessary to access, display, run or print my dissertation or thesis. I acknowledge that University of Arizona Library may elect not to distribute my dissertation or thesis in digital format if, in its reasonable judgment, it believes all such rights have not been secured. Signed: [signature] Date: 5-5-10

Last updated: Nov 15, 2009

Statement of Responsibilities:

Brian Bailey:	Microcontroller coding and wireless design
Brian Ebel:	LED driver design
Scott Galvin:	Optical design and photodiode research
Jack Grantham:	User interface design and coding
Scott Little:	LED driver design
Erica Morey:	Housing design, research on pulse oximetry
Joseph Sankman:	Transimpedance amplifier design
Christopher Stemple:	Team lead and manager and amplifier design

Joey Sankman

Date: 5-5-10

Development of a Remote Pulse Oximeter

Submitted by Team 4171:

Brian Bailey
Brian Ebel
Scott Galvin
Jack Grantham
Scott Little
Erica Morey
Joseph Sankman
Christopher Stemple

Submitted to:

Fred Highton (Mentor)
Matthew Hann (Sponsor)

Submitted on:

May 1, 2010

Interdisciplinary Engineering Design Program
University of Arizona

Frontispiece

The team members comprising the Remote Pulse Oximeter design group. Members on bottom row starting at left: Brian Ebel, Erica Morey, Joey Sankman, and Brian Bailey. Members on top row starting at left: Scott Galvin, Jack Grantham, Christopher Stemple, and Scott Little.

Abstract

Pulse oximetry is widely maintained as the standard method for measuring a person's blood oxygen saturation. Monitoring such a vital sign allows for detecting the onset and progression of various diseases and conditions that could result in tissue and organ damage or death due to lack of required oxygen delivery. The goal of this project was to design a pulse oximeter geared toward consumer use that could wirelessly transmit data to a portable device, such as a smartphone, for convenient, remote monitoring of oxygen saturation. This report describes the design process for developing a working prototype of the pulse oximeter. Texas Instruments sponsored this project for the Interdisciplinary Engineering Design Program at the University of Arizona. Their goal in funding this project was to develop an intimate knowledge base of the considerations, components, and overall design of a pulse oximeter in order to better assist their customers. The creation of the pulse oximeter reference design was inspired by thorough research on the scientific principles underlying pulse oximetry as well as existing pulse oximeter technologies. From the information collected, the team developed three potential designs for the device. Analysis of each design was conducted to distinguish the one design that would be further developed and fabricated into the working reference design required by the project sponsor. Results obtained by testing the final prototype, discussion of future directions for the reference design, and conclusions drawn from the completion of the project are also presented in this report.

Table of Contents

1 Introduction 8
2 Theory 9
2.1 Background & Assumptions 9
2.2 Principles of Pulse Oximetry 10
3 System Requirements 13
3.1 Accuracy 13
3.2 Battery Life 13
3.3 Perceptible Alert Signal 14
3.4 Data Logging 14
3.5 Transmission Distance 14
3.6 Shock Resistance 14
3.7 Water Resistance 15
4 Design Concepts & Analysis 15
4.1 Design 1 16
4.2 Design 2 17
4.3 Design 3 18
4.4 Concept Analysis 20
5 Final Design Breakdown 22
5.1 Theory of Operation 22
5.2 Subsystems 22
5.2.1 Housing 24
5.2.2 Source/Detector 27
5.2.3 LED Driver 29
5.2.4 Transimpedance Amplifier 34
5.2.5 Digital Interface 45
5.2.6 User Interface 47
6 System Build 51
6.1 Subsystem Testing 51
6.2 Subsystem Integration 53
7 System Testing 54
7.1 Housing Testing 55

7.2 LED Driver Testing 58
7.3 Transimpedance Amplifier Testing 59
7.4 Microcontroller Testing 61
7.5 User Interface Testing 62
8 Conclusions & Recommendations 63
9 Acknowledgements 65
10 References 66
11 Appendix A: Main Component List 67
12 Appendix B: Bill of Materials 68
13 Appendix C: Project Budget/Expenses 70
14 Appendix D: Housing Material Properties 71
15 Appendix E: Microcontroller Source Code 77

List of Tables

Table 1: System requirements specified by sponsor for final pulse oximeter design 13
Table 2: Pugh study for three design concepts 21
Table 3: Bits 1 and 0 of the pointing register which determine where the next read/write will occur 46
Table 4: Both bytes of the configuration register to be written to 46
Table 5: Subsystem testing procedures and results 52
Table 6: Testing equipment 53
Table 7: Overall system testing procedure and results 55

List of Figures

Figure 1: Typical pulse oximeter configuration [4] 10
Figure 2: Attenuation of oxyhemoglobin and deoxyhemoglobin with wavelength [5] 11
Figure 3: Representation of light absorption with time [8] 12
Figure 4: Design 1 - (Left) LED driver circuit. (Right) Driver current output 16
Figure 5: Design 2 - (Left) LED driver circuit. (Right) Driver current output 18
Figure 6: Design 3 - (Left) LED driver design. (Right) Driver current output 19
Figure 7: Block diagram showing final design by subsections 23
Figure 8: Sensor housing: (Left) Trimetric view, (Right) Cross-sectional view 25
Figure 9: Exploded view of sensor housing: (Left) Top/front housing arm. (Right) Bottom/back housing arm 25
Figure 10: Main housing: (Left) Exterior of housing, (Right) Exploded view showing components 26
Figure 11: Photo of completed prototype and iPod Touch used for interface 26
Figure 12: Infrared LED, red LED, and photodiode selected (left to right). Relative sizes are accurate. 27
Figure 13: Attenuation curve showing location of red and infrared wavelengths 28
Figure 14: LED driver block diagram 29
Figure 15: LED driver configuration 30
Figure 16: TINA LED driver circuit diagram 31
Figure 17: TINA simulation results: (Left) Voltage versus current. (Right) Pulse voltage versus current 31
Figure 18: LED current for variable input voltage 32
Figure 19: LED current for a pulsed signal 32

Figure 20: LED driver circuit with compensation: (Left) Circuit diagram. (Right) LED current for a pulsed signal 33
Figure 21: LED driver circuit with temperature sensor 34
Figure 22: Block diagram of analog frontend and adjoining components 35
Figure 23: (Left) Simple transimpedance amplifier. (Right) Compensated transimpedance amplifier 36
Figure 24: Gain curves for A_{OL} and 1/β 36
Figure 25: (Left) Transimpedance amplifier. (Right) Small signal transimpedance amplifier 37
Figure 26: Resistive tee network 40
Figure 27: Bootstrapping configuration 41
Figure 28: TINA circuit layout of the transimpedance amplifier 43
Figure 29: (Left) Frequency response of transimpedance amplifier. (Right) Transient response to 10nA, 500µs pulse 43
Figure 30: Noise analysis of transimpedance amplifier 44
Figure 31: Design template for user interface featuring 2 main screens 48
Figure 32: Final user interface GUI implemented on iPod Touch 48
Figure 33: User interface program flow 49
Figure 34: Full system flowchart 53
Figure 35: PCB layout for main housing board 54
Figure 36: SolidWorks FEA analysis performed on main housing unit 56
Figure 37: SolidWorks FEA analysis performed on LED arm of sensor housing 56
Figure 38: SolidWorks FEA analysis performed on photodiode arm of sensor housing 57
Figure 39: SolidWorks FEA analysis performed on photodiode cover 57
Figure 40: SolidWorks FEA analysis performed on cover for LEDs 57
Figure 41: Voltage across the LED driver drain resistor - used for current sensing 58
Figure 42: Red and infrared LEDs switching capability 59
Figure 43: Voltage output from transimpedance amplifier 60
Figure 44: AC ripple representing pulse rate 61
Figure 45: Final iPhone interface 62

1 Introduction

This report details the design, development, and construction of a remotely monitored pulse oximeter, a device that measures blood oxygen saturation. The project was offered as part of the Interdisciplinary Engineering Design Program at the University of Arizona. In this program, undergraduate seniors are grouped into design teams that are responsible for the completion of a project sponsored by one of several companies from industry. The teams have 30 weeks to develop and construct the device specified by the project sponsor. Texas Instruments (TI) was the sponsor of this project with Matthew Hann, an HPA Linear Applications Engineer for TI, as the company representative in charge of guiding the project and working with the student team during its development.

Texas Instruments designed this project such that the design team would assist them in an area where they lack technical expertise. TI is a world leader in the design and manufacture of analog, digital signal processing, radio frequency (RF), and digital light processing (DLP) technologies that other companies utilize in the development of electronic devices and equipment. Recently, they have had numerous customers interested in designing pulse oximeters and seeking expertise regarding component selection and design architecture. Since TI does not develop pulse oximeters themselves, they lack the technical knowledge in demand.

The project entailed the design of a pulse oximeter intended primarily for consumer use. This requirement meant that the device needed to be user-friendly and as small and unobtrusive as possible. Pulse oximeters for consumer use have been on the market for a number of years now; however, the novelty of this project was mostly in the remote monitoring capability of the oxygen saturation data. TI wanted a device that could incorporate and demonstrate some of the wireless technology it has developed, so the decision was made to have a pulse oximeter with the ability to communicate data to a smartphone or other portable device. This potentially made the device smaller by not needing to incorporate a display and user interface on the oximeter itself. It also lent itself to situations such as remote monitoring of an infant's oxygen levels during sleep to warn of dangerously low oxygen conditions that may be associated with Sudden Infant Death Syndrome (SIDS) or suffocation. However, the ultimate goal of the project was to develop a working oximeter prototype so TI could use it as a reference design. TI could then use the design and the knowledge accumulated throughout its development to better address the needs of their customers.

This report discusses the functional requirements specified by Texas Instruments for the design of the oximeter. It then outlines the three design concepts developed and considered, with emphasis on the development and analysis of the final design that was chosen for further scrutiny and construction. The details of each subsystem and the testing performed on each are discussed, as well as the integration of the components and the overall system testing. Testing results are shown and related to system functionality and the original functional requirements laid out for the project. Finally, discussion of results and concluding remarks about the project are made along with any recommendations for further development.

2 Theory

The science of pulse oximetry has been around since the mid 1970s. It was developed in response to a need for a real time, non-invasive method for measuring a person's blood oxygen saturation. The purpose of acquiring this data is to ensure that the wearer's ability to transport oxygen to the cells in his or her body has not been compromised. It is important for tissues and organs to receive substantial oxygen, because without it, they do not function properly and damage results. Lack of substantial oxygen delivery to any part of the body, called hypoxia, can be a primary symptom of many diseases or conditions, but it can also result any number of secondary symptoms depending on where it is occurring. Therefore, pulse oximetry is helpful for assessing a more direct cause of many symptoms in medical diagnostics. The specific low oxygen condition detected by pulse oximeters is called hypoxemia, which is characterized by hemoglobin oxygen saturation at or below 90%. Invasive oximeters (the first type to be developed) rely on taking an arterial blood sample from the patient and submitting it to the oximeter for analysis of blood gas levels. This process provides extremely accurate data; however, it is also time consuming, invasive, and only offers a snapshot of a person's blood gas levels, which can change very quickly. Pulse oximetry addressed these concerns by allowing for real time, non-invasive, continuous monitoring of oxygen saturation albeit with slightly lower accuracy and use limitations when compared with traditional, invasive blood gas analysis.

2.1 Background & Assumptions

Hemoglobin is a main component contributing to the composition of a person's blood. It is a molecule responsible for binding with the oxygen inhaled through the lungs and then transporting that oxygen through the blood stream to the body's tissues and organs. Hemoglobin that is bonded to oxygen is

called oxyhemoglobin (HbO_2) while hemoglobin that is not is termed deoxyhemoglobin (Hb). When the heart contracts, it pumps a fresh supply of oxyhemoglobin through the blood stream where the oxygen then diffuses down its concentration gradient into the cells of the body. Each pump results in a high concentration of oxyhemoglobin in the arteries. Each time the heart relaxes, the pressure in the arteries decreases along with the concentration of oxyhemoglobin. However, as one may suspect, this is a highly simplified overview of the processes occurring in the body.

In addition to the hemoglobin, called functional hemoglobin, which is able to bind with oxygen, it can also bind with other substances to form non-functional hemoglobin. These substances include most notably carbon monoxide, forming carboxyhemoglobin (HbCO) and methane, forming methemoglobin (METHb), for which the pulse oximeter does not account. When the heart contracts, all forms of hemoglobin present are being forced through the arteries, not just deoxy- and oxyhemoglobin. Pulse oximetry has an important limitation in that it makes the critical assumption that in normal functioning of the body there are very low levels of HbCO and METHb, which allows for a relatively simple percentage calculation involving only HbO_2 and Hb for measuring oxygen saturation levels. It assumes that the concentration of all hemoglobin types except deoxy- and oxyhemoglobin at any point in the body is constant and negligible as blood is pumped through the arteries with each relaxation and contraction of the heart. This most often reasonable assumption allows for a less complicated way of measuring blood oxygen saturation [4].

2.2 Principles of Pulse Oximetry

Typical pulse oximeters utilize two light emitting diodes (LEDs), one red and one infrared, to measure relative levels of HbO_2 and Hb as blood is pumped through the body. The LEDs are positioned on one side of an extremity of the body, usually a finger, ear or toe, and a photodetector is placed on the opposite side, as in Figure 1.

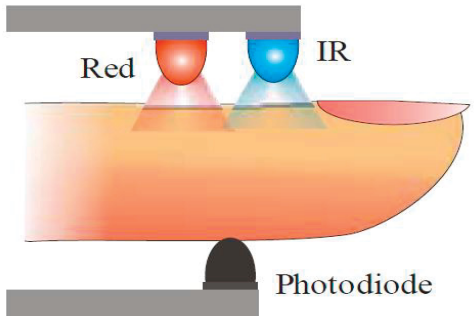

Figure 1: Typical pulse oximeter configuration [4]

In operation the LEDs are pulsed alternately, with one off while the other is on, allowing the photodetector to measure the transmitted light intensity at each wavelength separately. The transmitted light intensity differs greatly at each wavelength and can be attributed to the attenuation as it travels through the body, which results from a combination of reflection, scattering, and absorption by tissue and bone, venous blood, and arterial blood in the region. These values are then also related to the absorption of light by the oxyhemoglobin and deoxyhemoglobin molecules. Figure 2 shows the absorption of each molecule and its dependence on wavelength.

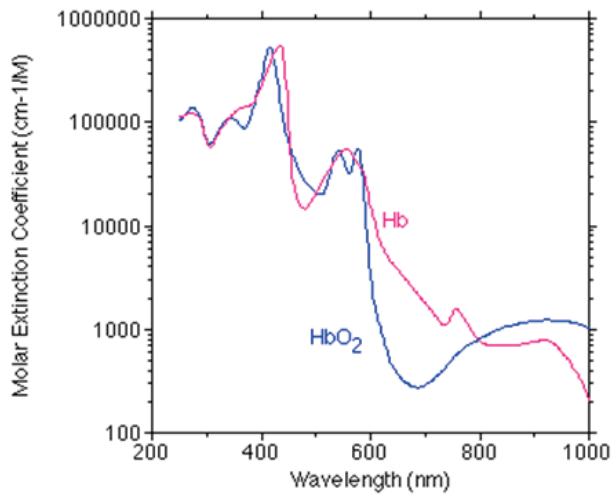

Figure 2: Attenuation of oxyhemoglobin and deoxyhemoglobin with wavelength [5]

The idea is that at the red wavelength (normally around 660 nm), the absorption by oxyhemoglobin ($Hb0_2$) is significantly less than for deoxyhemoglobin (Hb). Conversely, at the infrared wavelength (usually around 910 nm), the relationship switches, with HbO_2 absorbing more than Hb. This means that measuring the light output at these two wavelengths will differ greatly due to the concentrations and absorbance properties of each hemoglobin type. As stated before, as the heart contracts and relaxes, the concentration of HbO_2 fluctuates respectively, which causes the amount of light absorbed as it travels through the sample to change. This results in a cyclic relationship between absorption and time that takes the form shown in Figure 3, with the peaks and troughs corresponding to the beating of the heart as well as high and low oxyhemoglobin concentrations respectively.

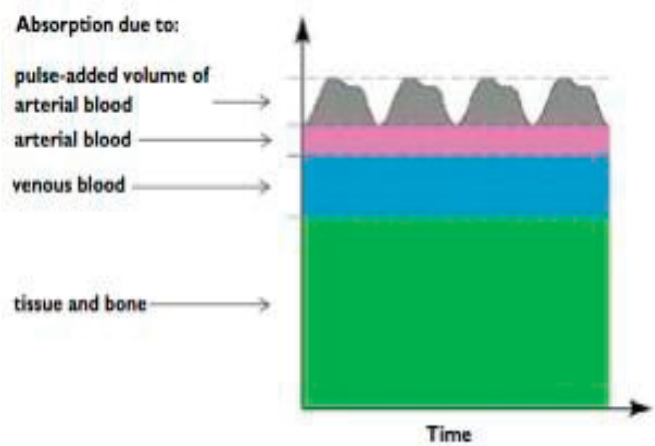

Figure 3: Representation of light absorption with time [8]

The corresponding transmitted light measured by the pulse oximeter at each wavelength will follow a similar pattern to the absorbance in Figure 3, but inverted. This is due to the inverse relationship between optical power and absorbance. The direct current (DC) component of the pulse oximeter signal is attributed to the aforementioned scattering, reflection, and absorption as the light passes through the sample, which is assumed constant. As such, the AC component is attributed solely to the changes in Hb and HbO_2 concentrations. By taking a ratio of the difference in the AC and DC components at each wavelength, the blood oxygen saturation can be estimated. The ratio (R) can be expressed by the relationship in Equation 1, where I refers to the current output by the photodetector [3].

$$R = \frac{\log_{10}(I_{DC+AC}/I_{DC})_{\lambda 1}}{\log_{10}(I_{DC+AC}/I_{DC})_{\lambda 2}} \tag{1}$$

Through calibration of the pulse oximeter, this ratio can then be related to actual blood oxygen saturation. Pulse oximeters are typically calibrated by comparing readings at specific times with data gathered from a blood gas analysis done at the same times and then mathematically relating the ratios to actual blood oxygen levels.

3 System Requirements

The project sponsor specified several requirements the final pulse oximeter design would need to meet. Table 1 shows a summary of those requirements along with several other characteristics relating to each condition. The importance of each requirement to the sponsor is shown on a scale of 1 to 5, with 5 signifying the most important. In addition, the metrics and target values used to objectively quantify the requirements are shown.

Table 1: System requirements specified by sponsor for final pulse oximeter design

Functional Requirement	Customer Importance	CTQ (metric)	Target Value
Accuracy	5	Percentage (%)	Accurate to within ±2% of actual blood oxygen concentration
Battery Life	5	Hour	Minimum of 12 hour battery life on a single charge
Perceptible Alert Signal	5	Decibels (dB)	80 dB
Data Logging	4	Week	1 weeks worth of data from continuous monitoring
Transmission Distance	4	Meter (m)	25 m wireless data transmission
Shock Resistance	2	Meter (m)	Survive at least 2 m fall
Water Resistance	2	Meter (m)	Water resistant to depth of 3 m

3.1 Accuracy

One of the most important aspects of any medical device is its accuracy. Inaccurate devices can generate false positives, potentially leading to medical action taken when it may not be required. Even worse, they may fail to detect or report a condition that could lead to serious health risks or even death. Therefore, the final pulse oximeter design was required to be accurate to within ±2% of the actual blood oxygen concentration of the user. This metric is comparable to the accuracy of many other pulse oximeters that are currently available and used in medical environments.

3.2 Battery Life

The pulse oximeter was developed for consumer use, and thus would require the potential to be worn throughout the night while the user slept. Consequently, the device needed to last a minimum of 12 hours on a single charge such that it would continue to function without need for attention while the user rested.

3.3 Perceptible Alert Signal

One of the novel aspects of the remote pulse oximeter design was the implementation of an alarm in the event that the blood oxygen level of the user fell below a safe level. The alarm needed to be loud enough to be heard throughout a typical household, but not so loud that it would damage human hearing. A target metric of 80 dB was chosen for the pulse oximeter alarm due to it being a nice balance between normal human conversation (60-65 dB) and the human pain threshold (125 dB).

3.4 Data Logging

In order to monitor trends in the blood oxygen saturation of the user, a means to record and store data was integrated into the final pulse oximeter design. A metric of one week's worth of continuous oxygen saturation data being able to be stored and accessed was chosen in order to give the user ample time to back up the data to an external source, such as a hard drive or home computer. It was proposed that the device would output a file that was easily accessible and readable using common software, such as Microsoft Excel, so that both the user and medical personnel alike could easily read and analyze the recorded blood oxygen levels over long periods of time.

3.5 Transmission Distance

A wired design limits how a pulse oximeter can be used and where it can be located on the body. To alleviate these constraints, the design of the remote pulse oximeter included a unique feature, the ability to transmit information wirelessly to a portable device such as an iPod or iPhone. The average American home is approximately 2300 square feet in size [10]. By assuming the average house is three times longer than it is wide, this corresponds to a length of 83 feet or 25 meters. This led to the chosen transmission distance metric of 25 meters for the design.

3.6 Shock Resistance

The physical construction of the pulse oximeter needed to be durable enough to handle the daily rigors of being worn by an adult or child. Therefore, it was desired that the final product have a measurable level of shock resistance. Since the device was intended to be worn by a person, and it was reasonably assumed the device would suffer only normal abuse, the shock it would need to withstand was that of a fall from the height of a typical person. Thus, the conservative target metric of maintaining functionality after a two meter fall was chosen.

3.7 Water Resistance

The two most realistic concerns in relation to water resistance were that the device may end up either in a bathtub of water, or experience some sort of wet environment from human sweat or saliva from an infant. In consideration of these conditions, and given that it is the common metric for a wristwatch, a target metric of water resistance to a depth of 3 meters was imposed on the pulse oximeter design.

4 Design Concepts & Analysis

Accompanying the functional requirements specified by the sponsor, there were several important considerations that went into the development of the possible pulse oximeter designs. One consideration, which was also a functional requirement, was that the oximeter needed to operate solely on battery power for at least 12 hours. This meant the electronic design and components selected needed to result in low power consumption in order to meet the requirement. Another point to consider was the oximeter being developed for consumer use. This required that the device be relatively small and as unobtrusive as possible, while also being comfortable and convenient for the user to wear throughout prolonged periods of use. The last major consideration was the accuracy requirement for the device. This meant the location used to measure the oxygen saturation needed to be carefully selected, and the design of the electronic components needed to be stable enough to ensure the device would meet the specified accuracy of ±2%.

In each of the following system designs there are four parts: the source/detector, the LED driver, the signal amplifier, and the digital/user interface. The source is a combination of two LEDs, one red and one infrared, which are pulsed at alternate times. The detector consists of a photodiode located opposite the two LEDs, which detects the amount of light passing through the tissue. The LED driver is a circuit coupled with a temperature sensor and is used to manipulate the brightness and on/off state of each LED. The signal amplifier circuit amplifies the small currents generated by light incident on the photodiode to a usable signal. The digital interface is the circuit brain – it includes the microcontroller and its programming, which directs the functionality of the entire circuit. The digital interface also includes the wireless transmitter that sends data to the user interface. The user interface is the means by which the user can monitor his heart rate and oxygen saturation levels. The three system designs initially considered are summarized in the following sections.

4.1 Design 1

The first design the team developed consisted of an oximeter that would be placed on the finger of the wearer. Two LEDs would be used for the source, one red and one infrared, and an avalanche photodiode (APD) utilized as the detector. An APD can be thought of as a photodetector that provides a built-in first stage of gain through avalanche multiplication, which is regarded as the semiconductor analog to photomultiplier tubes. The trade-off to obtain this gain is that a large reverse-bias voltage must be present across the APD. Furthermore, a Fresnel lens would be placed above the APD to collect as much of the light as possible that was transmitted through the finger.

The LED driver circuit for this design is shown in Figure 4. This design places the LEDs on the collector of the NPN transistor shown. This implementation uses a small number of components and offers low power consumption and low current drift. The feedback loop around the operational amplifier provides stability by reducing the current drift on the output. A downside to the design is that there is an overshoot present on the output current (see Figure 4 at right). This overshoot will make the max current of 100mA difficult to get exactly because if the input voltage is slightly under or slightly over, the current will be below the 100mA. This also presents a possibility that the transistor could become too hot since it would be driving all the current.

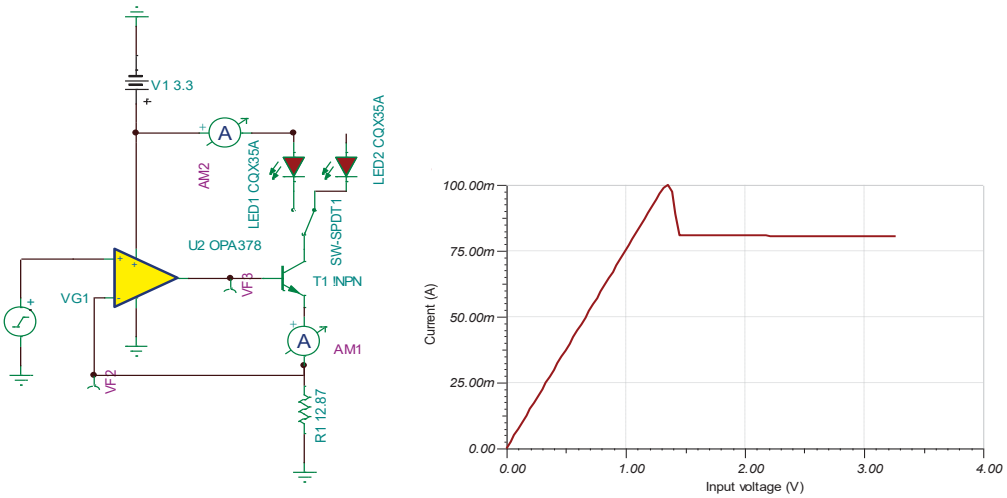

Figure 4: Design 1 - (Left) LED driver circuit. (Right) Driver current output

The signal amplifier would rely on a standard operational amplifier (op-amp) design with a voltage to voltage amplification structure using a photoconductive operation. A photodiode in photoconductive mode is operated in reverse-biased conditions, reducing the junction capacitance. This would be a low power design offering high speed and sensitivity. However, the voltage generated by the photodiode would be extremely small and extremely difficult to resolve with a high level of precision. In addition, the increased sensitivity would lead to higher noise. Due to the very small voltage levels and high sensitivity, this design would result in higher noise and lower signal strength, thus making it less accurate than other designs.

The interface design of the system would consist of the pulse oximeter transmitting via WiFI to the Internet where it would then be accessible to any web-capable device. This design offers the flexibility that any web-capable device could access it; however, it would also be complex to implement and consume a large amount of power.

4.2 Design 2

The second design that the team developed was also for use as a finger-mounted pulse oximeter. The source design was the same, consisting of two LEDs, one red and one infrared. A phototransistor was selected for the detector, as it would provide internal gain. To increase the light collection capability, a reflective light collector made of either glass or plastic would be placed on top of the detector. This design would increase the light collection efficiency, thereby decreasing the power consumption of the system, but unfortunately it would be fairly large and bulky due to the size of the light collector.

The LED driver circuit for this design is shown in Figure 5. This design places the LEDs on the output of an AB power output stage. This allows the current to go both directions depending on the input voltage. If the input voltage is high or positive then the top NPN transistor will be on, pushing the current out and turning LED 1 on. If the input voltage is low or negative then the bottom PNP transistor will be on, pulling the current and turning LED 2 on. The feedback enables this transition to not have what is called a dead zone, or a small region in the middle in which both transistors are off at the same time. This circuit is advantageous because it enables a very stable linear output current, it does not need a switch, and it allows the two transistors to have all of the current so one does not heat up. Some of the main problems are that this circuit will draw more power than the previous design, and it is a larger overall circuit. Another issue is that this circuit needs ±5V power supply, but only a 3V battery was specified for use.

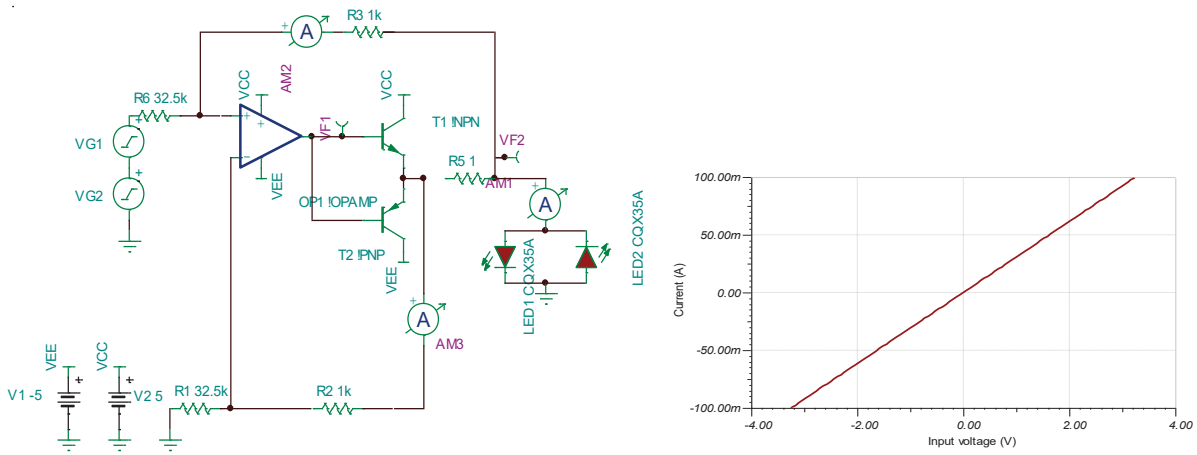

Figure 5: Design 2 - (Left) LED driver circuit. (Right) Driver current output

The signal amplifier would rely on current to current amplification structure using a photovoltaic operation. Photovoltaic operation has no reverse-bias on the photodiode. This would be a low noise, low power design that would also offer direct amplification of the signal from the photodetector. However, the current output from the amplifier would then need to be converted to a voltage for the analog-to-digital converter. If dissipated through a resistor to produce a voltage, this would constitute an unreasonable waste of power to create a voltage signal. If a small resistor is used to dissipate the current to save power, and a voltage amplifier is used to condition the signal for analog-to-digital converter, the purpose of a current to current amplifier would be defeated. Thusly, a current to current amplifier would be an inefficient option.

The method of wireless transmission chosen for this design was Bluetooth. Transmission of the data to a portable device using Bluetooth would be the simplest to implement and allow for a direct connection to the device. The downside would be that only Bluetooth compatible devices could receive the signal, and that Bluetooth also consumes a large amount of power.

4.3 Design 3

The third design considered, and the one ultimately chosen to proceed with development, consisted of a pulse oximeter sensor fastened to the ear of the wearer. This offered an advantage over the proposed finger oximeters because a person generally moves their ears much less than their fingers. This would reduce motion artifact within the signal, which would increase the accuracy of the oxygen saturation read out from the pulse oximeter. The downside to this design was that the housing was more complex in order to make it more comfortable for the wearer.

Due to the small size requirements of the ear-oximeter housing, the source and detector design was restricted to being relatively simple. Again, two LEDs would be used for this design, one red and one infrared. However, for the detector a PIN photodiode would be used for its relatively high responsiveness and low dark current. Furthermore, the photodiode would not need to be reverse-biased to operate which would result in a lower power design. No optics could be feasibly used due to the size restrictions on the housing.

The LED driver circuit for this design is shown in Figure 6. This circuit is similar to that in Design 1; however, it uses a PNP transistor with positive feedback instead of the negative feedback method used in Design 1. The positive feedback helps stabilize the current drift of the LED driver, but the PNP transistor allows a larger voltage drop across the LEDs because the output from the operational amplifier can be about 700mV below the 3V rail. Also, the collector of the PNP will allow the voltage to be above the base, thus the voltage above the LEDs can be close to 2.8V. This provides a larger voltage swing for the LEDs, whereas the NPN transistor would only allow about 2.1V. This promotes a higher accuracy of the output current since it allows for a larger input voltage swing and because there is no overshoot on the current. This allows any voltage above the maximum to achieve a maximum current of 100mA. This circuit still introduces the concern that only one transistor is being used to drive all of the current, leading to the possibility of it becoming too hot. Also, this design requires a switch to alternate between each LED. Overall the smaller size and power consumption makes it better than Design 2, as well as not needing a ±5V power supply. It also offers a desirable linear output current, similar to that of Design 2.

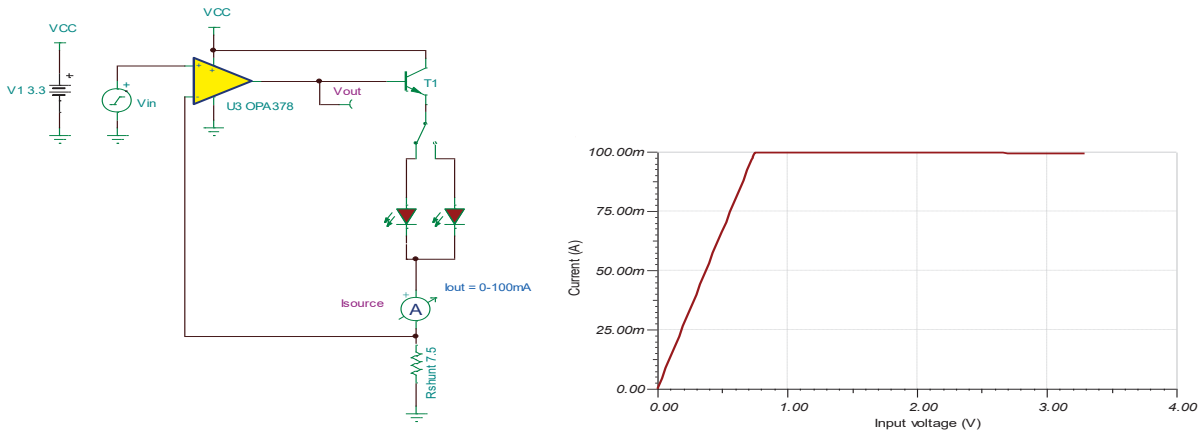

Figure 6: Design 3 - (Left) LED driver design. (Right) Driver current output

The signal amplifier design was based on a current to voltage amplification structure using a photovoltaic operation of the photodiode. This design allowed for direct amplification of the photodiode current while producing a voltage output for the analog-to-digital converter. This was a major advantage over Design 2 in that it eliminated the need for a second stage or the need for significant dissipation of power through a resistor. By amplifying the current through the photodiode instead of the voltage across it, a significant improvement in the signal-to-noise ratio was achieved in comparison with Design 1. Low noise and low power consumption are also benefits of this type of design, but the trade-off is the speed and sensitivity of the device.

The interface for the design was similar to that proposed for Design 1. The pulse oximeter would transmit data wirelessly via radio frequency (RF) to a base station and then the base station would transmit via WiFi directly to a portable device such as an iPod or iPhone. This design would benefit from low power consumption and easier implementation than the other designs.

4.4 Concept Analysis

After the three potential design concepts had been developed, it was necessary to devise a way of comparing the three designs in order to select the most promising design with which to move forward. This requirement led the team to conduct extensive research into the individual components and technologies outlined in the descriptions of each design concept. By researching the pros and cons of each design through trade studies, component specification comparisons, and computer modeling of component performance, the Pugh chart shown in Table 2 was developed.

The Pugh chart outlines the major characteristics of each design component that were considered and compared during the analysis. Each characteristic of each design was assigned a score from 1 to 5, with 5 meaning the design most desirably satisfied the requirement and 1 meaning the design least desirably met the requirement. Furthermore, each characteristic was weighted by importance also using a value between 1 and 5, with 1 representing low importance and 5 representing high importance. In order to compare the three designs overall, a weighted total of all characteristics for all three designs was calculated and is shown at the bottom of the chart.

Table 2: Pugh study for three design concepts

Design Parameter	Characteristic	Importance (1-5)	Design 1	Design 2	Design 3
Oximeter Location on Body	Design Simplicity	3	4	4	2
	Accuracy	5	3	3	5
	Cost	2	3	3	3
	Form Factor	1	4	4	2
Source/Detector	Design Simplicity	3	3	1	5
	Cost	2	1	3	5
	Power Consumption	4	2	3	4
	Sensitivity	3	5	4	3
LED Driver	Design Simplicity	3	4	2	4
	Cost	2	5	3	5
	Accuracy	5	3	5	5
	Sensitivity	3	2	4	4
	Power Consumption	4	4	3	4
Amplifier	Design Simplicity	3	4	3	5
	Cost	2	5	5	5
	Noise	5	3	4	5
	Accuracy	5	3	3	5
	Sensitivity	3	5	4	4
	Power Consumption	4	5	2	5
Interface	Design Simplicity	3	3	4	5
	Cost	2	3	3	4
	Transmission Distance	3	3	2	5
	Reliability	3	4	4	4
	Power Consumption	4	3	3	5
		Weighted Total	**265**	**253**	**341**

By analyzing the results of the Pugh study, Design 3 proved to be the most desirable design option based on the requirements outlined for the project. It received a final weighted score of 341, which was 76 points above the second strongest design concept. This confirmed the team's suspicion that Design 3 would be the most viable design with which to move forward. Hence, it was decided that Design 3, the ear-mounted pulse oximeter, would be the design that was further developed into a working prototype. The following section of this report describes in detail how the individual subsystems of this design were developed and implemented.

5 Final Design Breakdown

As stated previously, the final design selected for further development and construction was an ear-mounted pulse oximeter. This design allowed for the oximeter to be placed in an unobtrusive location, conveniently allowing the wearer to use his or her hands and conduct him or herself normally. The placement also helped reduce the signal noise due to motion artifact, thereby increasing the detection accuracy. Despite these advantages, the details of the pulse oximeter prototype design needed careful consideration due to the very small size requirement, making it more challenging to meet the functional requirements of the project. The details of final design are discussed in the sections that follow.

5.1 Theory of Operation

The operation of the ear oximeter was to closely follow that of standard pulse oximeters currently on the market. Therefore, it would consist of a red and an infrared LED placed on one side of the ear and opposite a photodiode. The LEDs would be pulsed, with one being on while the other is off and continually alternating in that fashion, at a combined rate of 100 Hz. Light would reach the photodiode, causing it to output a signal, which would then be amplified, processed, and the ratio of the two signals would be mathematically related to the actual oxygen saturation of the user. Afterward, the device would transmit the oxygen saturation as well as the pulsatile signal to an iPhone or iPod Touch and be displayed on a user interface that would allow the data to be monitored and stored.

5.2 Subsystems

The design of the pulse oximeter can be broken down into several subsystems. The subsystems and their interactions are visualized in the block diagram depicted in Figure 7. Within the housing of the ear-oximeter there are three main systems: the LED driver control, analog signal processing, and digital signal processing systems. The user interface is located outside the housing on a portable device and receives data wirelessly from the pulse oximeter.

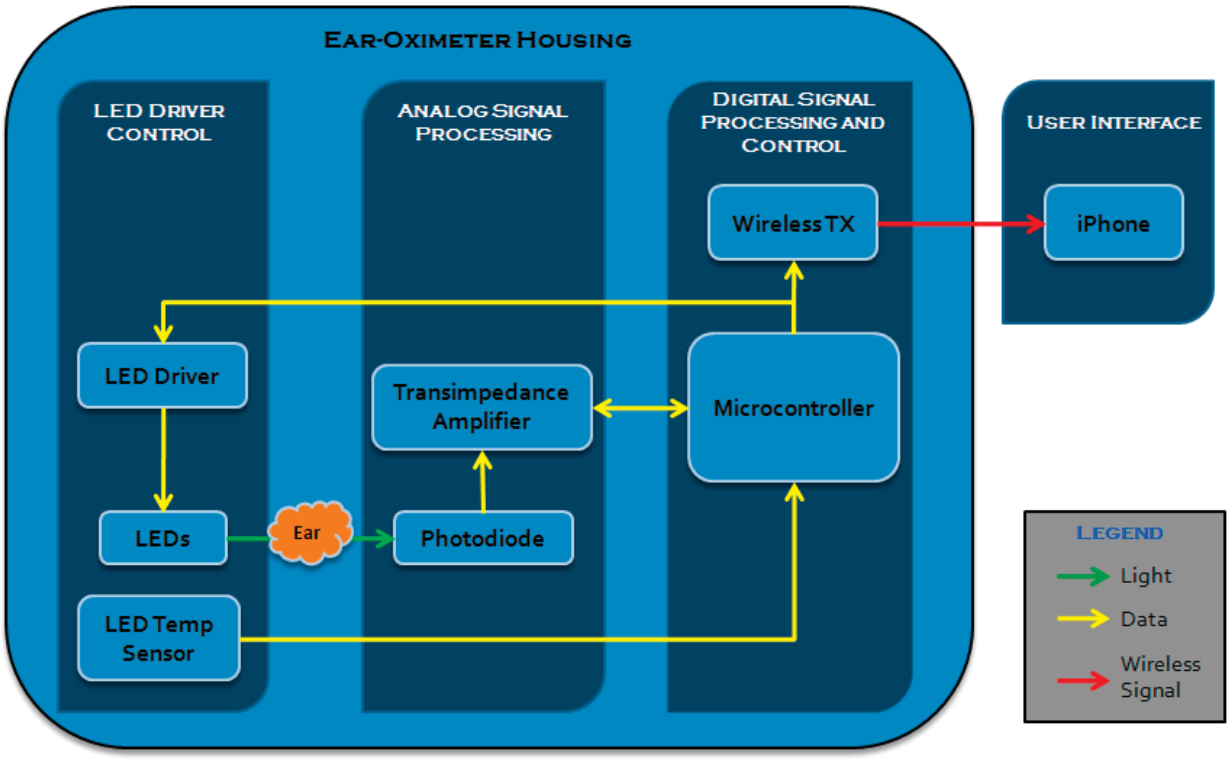

Figure 7: Block diagram showing final design by subsections

The microcontroller is the central unit controlling the functionality of most of the other systems. It sends signals to the LED driver, which adjusts the current going through the LEDs to produce a consistent and accurate light output. The photodiode senses the optical power (light) present on the other side of the sample (the ear in this case) and proportionally produces a current. This signal, in the form of an electrical current, is then sent to the transimpedance amplifier where it is converted into a voltage and amplified. The amplified signal is sent to the microcontroller where the signal data is processed and then sent to the wireless transmitter. The transmitter wirelessly communicates with the application on the iPhone to send and display the data on the user interface. There is also an LED temperature sensor in the housing that monitors the temperature of the LEDs and communicates with the microcontroller to adjust the current to the LEDs if the temperature near the skin rises to dangerous levels.

5.2.1 Housing

The pulse oximeter housing was divided into two main parts: the main circuitry housing and the sensor housing. The main housing contained the LED driver circuit, temperature sensor, microcontroller circuit, antenna, and battery, while the sensor housing contained the LEDs, photodiode, and signal amplifier circuit. Two separate modules were needed for several reasons. First, during design integration of the circuitry for the oximeter, it was discovered that the printed circuit board (PCB), in order to accommodate all of the circuitry, required the housing to be larger than originally anticipated. As a result, an ear-mounted housing would have been uncomfortably large. Furthermore, the team was initially planning to create an ear sensor as well as a finger sensor as interchangeable attachments, and this modular design would have allowed for the main housing to be used with each sensor without redesign. Given the cost of just one sensor housing and the unforeseen expenses incurred with regard to the PCBs, only the ear sensor was constructed.

Both housings were originally to be made of engineering plastic such as acrylonitrile butadiene styrene (ABS) or polycarbonate (PC). However, given the tight timeline and budget for this project, the team decided to use thermoplastic materials that mimic engineering plastic properties, supplied and suggested by 360 Prototyping, a rapid prototyping company located in Round Rock, Texas. Two different materials were required for the housings, a hard plastic for the shell of each housing and a rubbery material for the sensor housing where it would make contact with the ear. The rubbery pieces were fabricated using a material called TangoPlus – FullCure®930. The shell of the two housings was made using solid-state stereolithography (SLA) and a material called Accura®25, which has the look and feel of polypropylene (PP). The pertinent properties of both materials are given in Appendix D: Housing Material Properties. All parts of the housing needed to be dyed black to prevent ambient light from polluting the photodiode signal.

As stated previously, the sensor housing was designed to mount comfortably on the ear and contain the LEDs, photodiode, and amplifier circuitry. A 3-D model of the sensor housing design and cross-sectional view is shown in Figure 8.

Figure 8: Sensor housing: (Left) Trimetric view, (Right) Cross-sectional view

The sensor housing is made of two arms connected by a pin and spring. The pin allows the two arms of the housing to rotate, and the spring adds the perfect amount of tension, allowing for adjustment of the opening between the arms for application to and removal from the ear of the wearer (similar to the operation of a hair clip). The top/front arm of the sensor housing contains the PCB with the two LEDs mounted to it. The bottom/back arm of the housing contains the PCB with the transimpedance amplifier and the photodiode. An exploded SolidWorks model view, displaying housing arms, the pin and the PCBs, is shown in Figure 9. The PCBs are shown in green and the two rubbery pieces that contact the ear are depicted in black between the two PCBs.

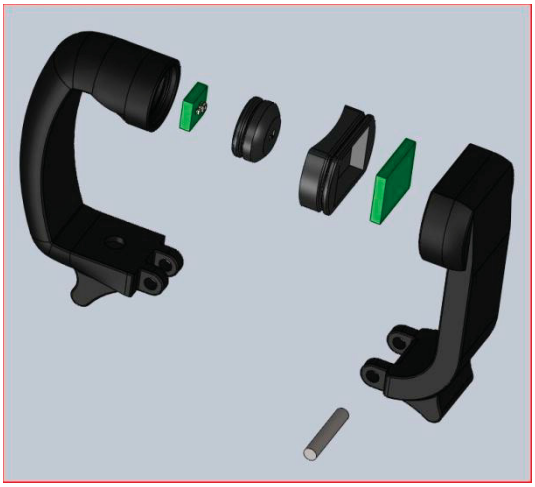

Figure 9: Exploded view of sensor housing: (Left) Top/front housing arm. (Right) Bottom/back housing arm

The main housing, accounting for its size, was mounted on the upper arm similarly to a portable music player. Figure 10 shows a 3-D model of the main housing. In the image at left, two bars are visible that run the length of the housing but are offset from the main unit. These bars will allow for an adjustable armband to be threaded through them in order to mount the device comfortably. The exploded view shows the lower compartment where the battery is housed and a view of the front compartment containing the main PCB, which consists of the temperature sensor, LED driver, microcontroller, and wireless transmitter.

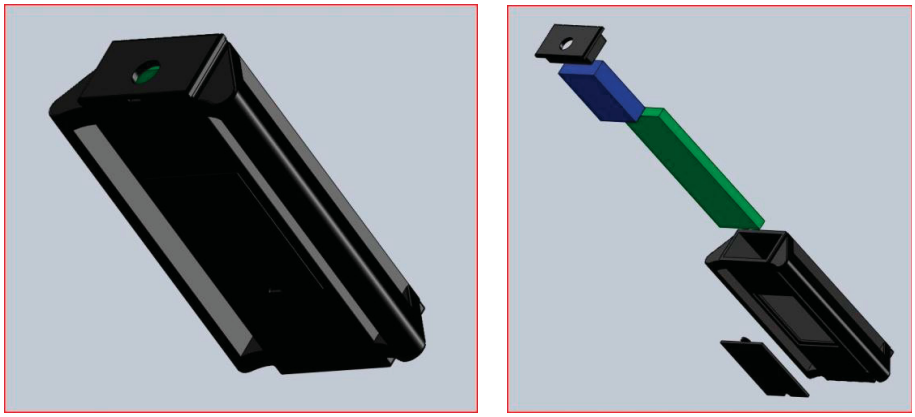

Figure 10: Main housing: (Left) Exterior of housing, (Right) Exploded view showing components

To connect the two housings, a 26 gauge wire was inserted into the sensor housing and soldered to the PCBs, while the free end of the wire terminated in a male flexible printed circuit (FPC) connector. This connector was plugged into a corresponding female FPC connector embedded in the main housing and connected to the PCB contained within. A photo depicting both prototyped housings and the wire connecting them is shown in Figure 11.

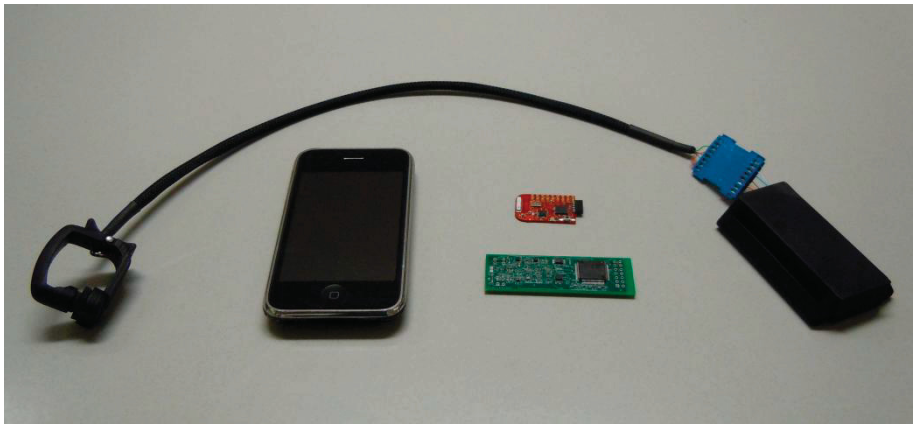

Figure 11: Photo of completed prototype and iPod Touch used for interface

5.2.2 Source/Detector

The source and detector design chosen for the ear oximeter is commonly used in standard pulse oximeters on the market today. Since the ear was to be used to measure oxygen saturation, the device needed to be as small and as lightweight as possible. This meant that the LEDs and photodetector selected needed to be as small as possible. This constraint also made it nearly impossible to include any sort of light collection optics to enhance the power output of the photodetector. However, due to the fact that the thickness of the ear in the site chosen is so small when compared to a finger or toe, the additional collecting optics were not necessary because plenty light would be incident on the photodetector without their use.

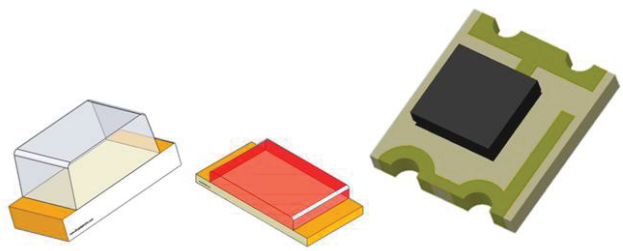

Figure 12: Infrared LED, red LED, and photodiode selected (left to right). Relative sizes are accurate.

With the aforementioned in mind, the LEDs chosen for the oximeter were a red LED with a peak wavelength of 650 nm and an infrared LED with a peak wavelength of 940 nm (see Figure 12). The red wavelength is located where the difference between the attenuation of oxyhemoglobin and deoxyhemoglobin is large, but not too large, otherwise not enough light would be incident on the photodetector (depicted in Figure 13). Likewise, the infrared wavelength was also chosen to have a large difference between the two attenuations but with the opposite sign. Choosing the wavelengths in this fashion would allow for a larger difference between the output signals at each wavelength, resulting in a more accurate calculation of the ratio of the two signals and thus the oxygen saturation level.

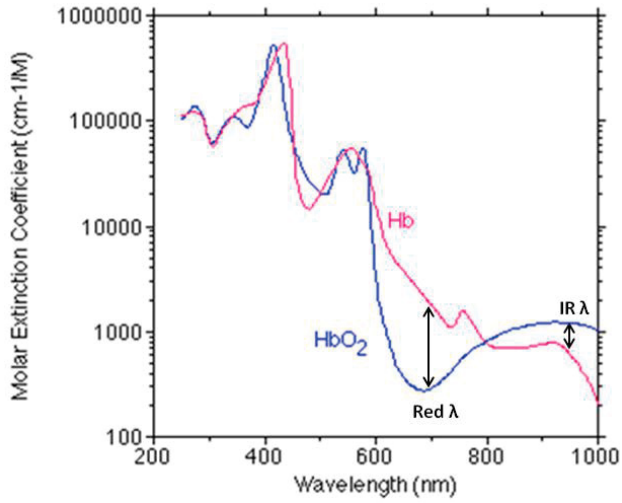

Figure 13: Attenuation curve showing location of red and infrared wavelengths

The LEDs were chosen for their high luminous intensities to allow as much light to be transmitted through the ear as possible, resulting in a higher signal output before amplification. They were also fabricated with a small footprint (approximately 1.5 mm by 0.8 mm) and low voltage and current requirements in an attempt to reduce the overall power consumption of the device. The LEDs were mounted in the housing next to each other on one side of the ear and directly opposite the photodetector.

As previously stated, the photodetector used was a silicon PIN photodiode. This was selected due to its high responsivity to both visible and near infrared wavelengths and its photovoltaic operation, again allowing the device to operate with lower power consumption. As with the LEDs, the footprint of the photodiode was also very important. However, this requirement also needed to be balanced with an active area that was as large as possible in order to collect the maximum amount of light possible. With these constraints in mind, the photodiode chosen has a small footprint of approximately 3.2 mm by 2.7 mm while maintaining a fairly large active area of 2.37 mm^2. The relative sizes between the photodiode and LEDs is shown in Figure 12. The manufacturers and part numbers for all components are available in Appendix A: Main Component List.

5.2.3 LED Driver

The main purpose of the LED driver was to produce a stable current to the two LEDs at separate times for a linear input voltage from the microcontroller. A typical LED driver block diagram is shown in Figure 14. TI specified that the LED driver needed to not only produce a stable current, but also have this current be variable from 0 to 100mA in order to decrease or increase the LED brightness as needed. Furthermore, the device was constrained to operating by means of a 3V Li-Ion battery which needed to be considered during design of the circuitry. If time permitted, TI also wanted a temperature sensor to be integrated with the LED driver to the possibility of burning a user as well as to keep the LEDs stable as high temperatures would cause the peak wavelength output to drift, affecting the oxygen saturation measurement.

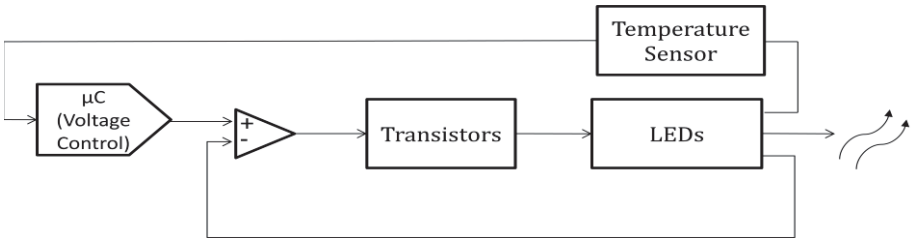

Figure 14: LED driver block diagram

The LED driver design depicted in Figure 15 shows the general circuit that was designed and used in the final prototype. The digital to analog converter (DAC) is controlled by the microcontroller to give different input voltages to the driver. The amount of current flowing through the LEDs is determined by this input voltage in a linear fashion, so as the input voltage increases so does the LED current. The feedback design of the LED driver along with the low voltage, zero drift operational amplifier being used (TI part OPA333) eliminates any current drift that would normally arise in the circuit.

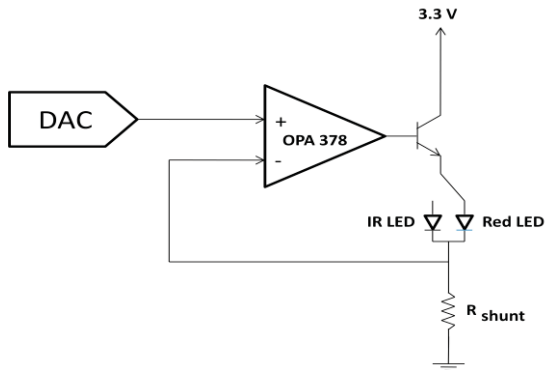

Figure 15: LED driver configuration

By nature of the operation amplifier, there is almost zero current in the feedback loop allowing the current through the LEDs to be determined by using the formula in Eq. 2.

$$I = \frac{V}{R} \tag{2}$$

The capability of the LED driver to deliver a variable current is very important for several reasons. For example, the LED brightness would need to be adjusted depending on the amount of fatty tissue present, the skin pigmentation, the bone density, as well as to reduce current to the LEDs if the temperature sensor reads that the LEDs are becoming too hot. Thus, it was crucial that the LED driver be able to produce a linear output current as the design in Figure 15 does.

To predict the operation of the LED driver circuit before a prototype was created, a circuit simulation program called TINA and provided by Texas Instruments was used. Figure 16 shows a circuit diagram of the LED driver as created with the TINA simulation software. The label V_{cc} present in the figure represents the constant voltage from the battery while V_{in} is the variable input voltage from the microcontroller and R_{shunt} is the resistor. The value of R_{shunt} dictates the amount of current that flows through the LEDs.

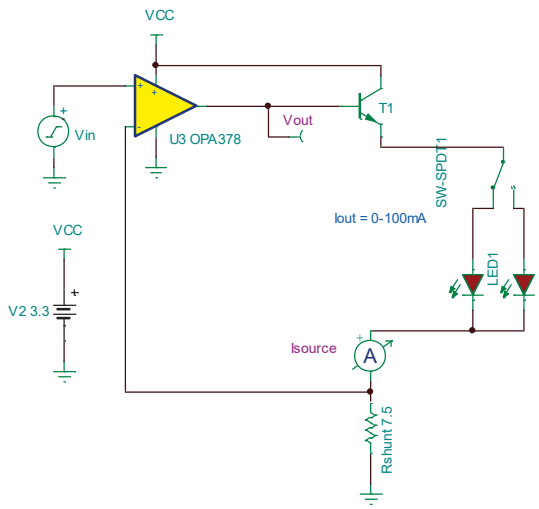

Figure 16: TINA LED driver circuit diagram

Figure 17 shows the TINA simulation results. The plot on the left depicts the current that passes through the LEDs as the voltage input from the microcontroller is varied. The plot on the right shows that with a pulse present on the input, there is a rise time and a fall time for the current through the LEDs, but it is very small. The simulation showed that the circuit operated as was expected, with a variable output current from 0 to 100mA and the ability for the red and infrared LEDs to pulse at separate times.

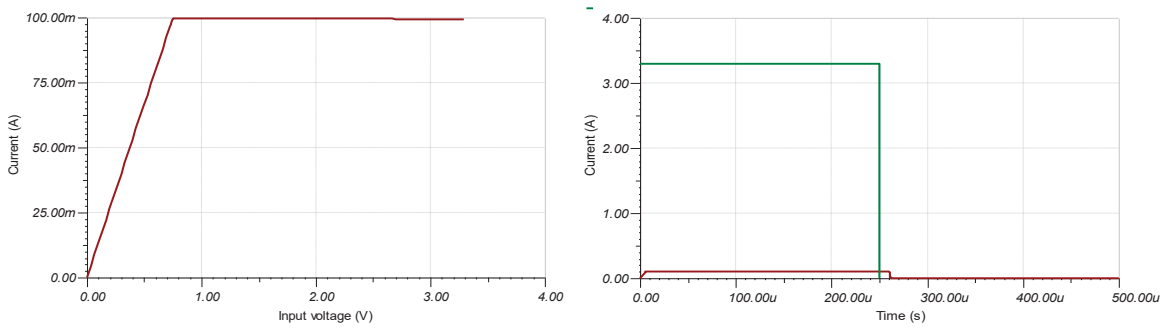

Figure 17: TINA simulation results: (Left) Voltage versus current. (Right) Pulse voltage versus current

The next step was to breadboard the circuit and see if similar results could be obtained to those predicted by the simulation. Figure 18 shows the results of the breadboarded circuit. The output current was linear as was predicted and desired. As the plot shows, the current did not go to 100mA due to the fact that the LEDs were not pulsed during this particular test. Therefore, the maximum current shown is near 25mA because this is the maximum current that the LED can run on at a constant voltage.

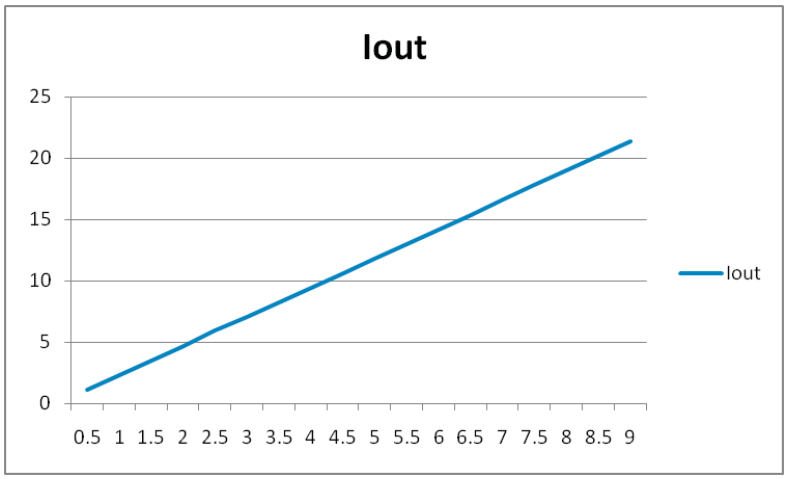

Figure 18: LED current for variable input voltage

The major discrepancy between the simulated results and those obtained while breadboarding the circuit arose when the LEDs were pulsed. Figure 19 shows that there were oscillations in the LED current (blue line) with a pulsed signal (orange line). The signal should have been a straight line instead of a saw-tooth curve. This test showed that the LED driver was not stable as was expected from the simulation. The oscillations showed the design was only marginally stable, and would need to be compensated.

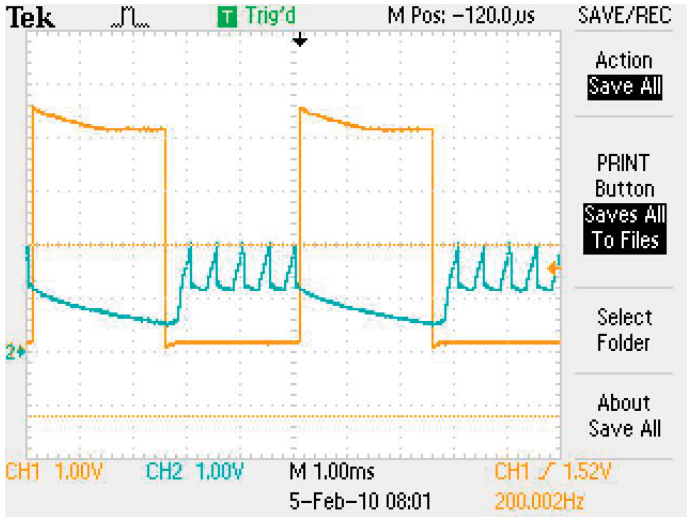

Figure 19: LED current for a pulsed signal

The circuit shown in Figure 20 (on left) shows the compensation that was added to the circuit to handle the oscillation in the output current. The circuit also has the LEDs in a back-to-back configuration to allow testing with a commercial Nellcor finger sensor. Adding the back-to-back configuration added an extra switch into the circuit. To accomplish the switching needed for this design, a quad switch TS3A44159 was used from Texas Instruments. The circuit was then assembled and tested on a prototype board. When tested, the oscillations in the LED current were no longer visible (refer to Figure 20 on right), only a clean output current was present. The circuit does have a small rise and fall time, but that was expected and should not affect the overall performance of the pulse oximeter.

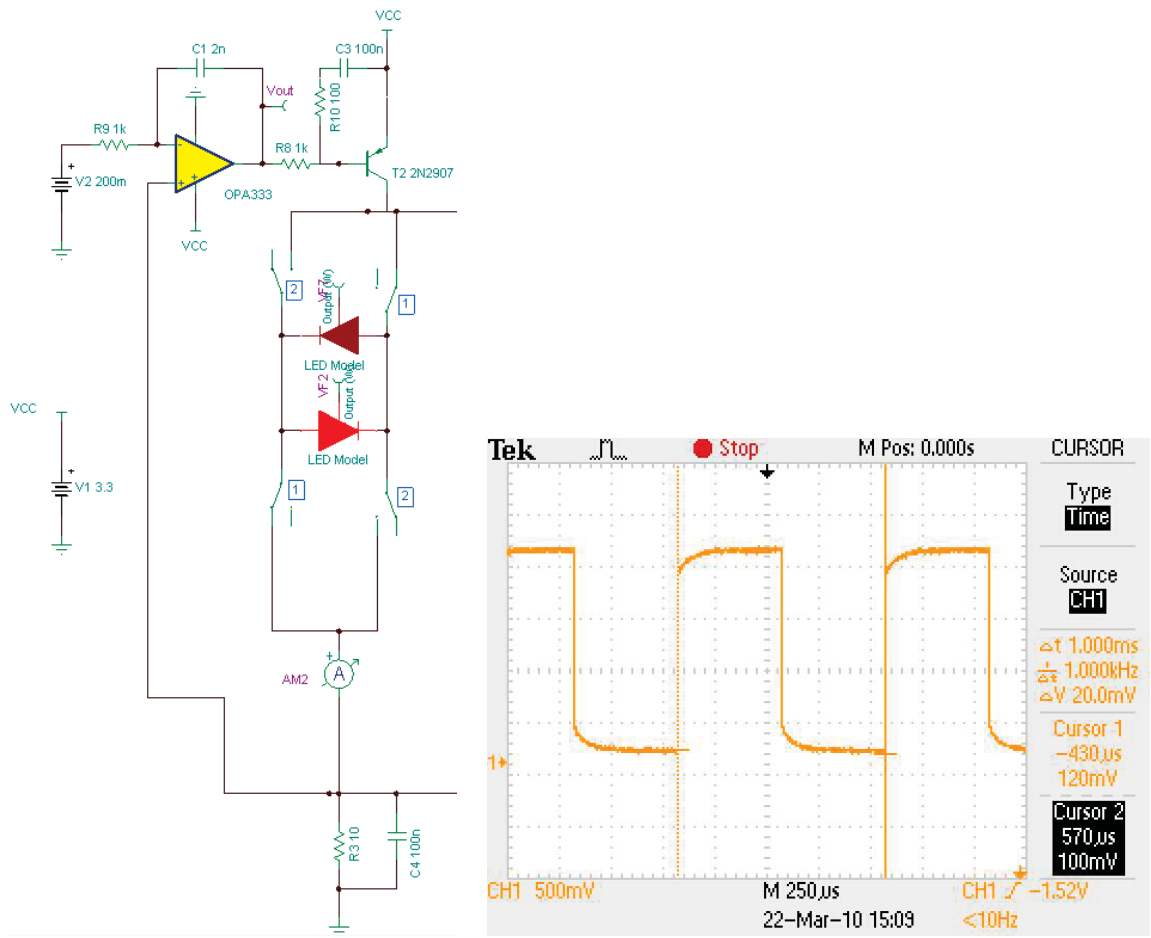

Figure 20: LED driver circuit with compensation: (Left) Circuit diagram. (Right) LED current for a pulsed signal

The last step in the LED driver design was to incorporate the temperature sensor with the driver circuitry. Figure 21 shows the resulting design of the circuit. The temperature sensor chosen was the TMP411. It works by sending a small current across the LED and measuring the voltage drop across it.

The sensor then computes the temperature of the LED based upon the measured voltage drop and the emission coefficient of the LED. The microcontroller was used to store the emission coefficients for each LED (red and infrared) and feed those values to the TMP411 when the appropriate LED temperature needed to be determined.

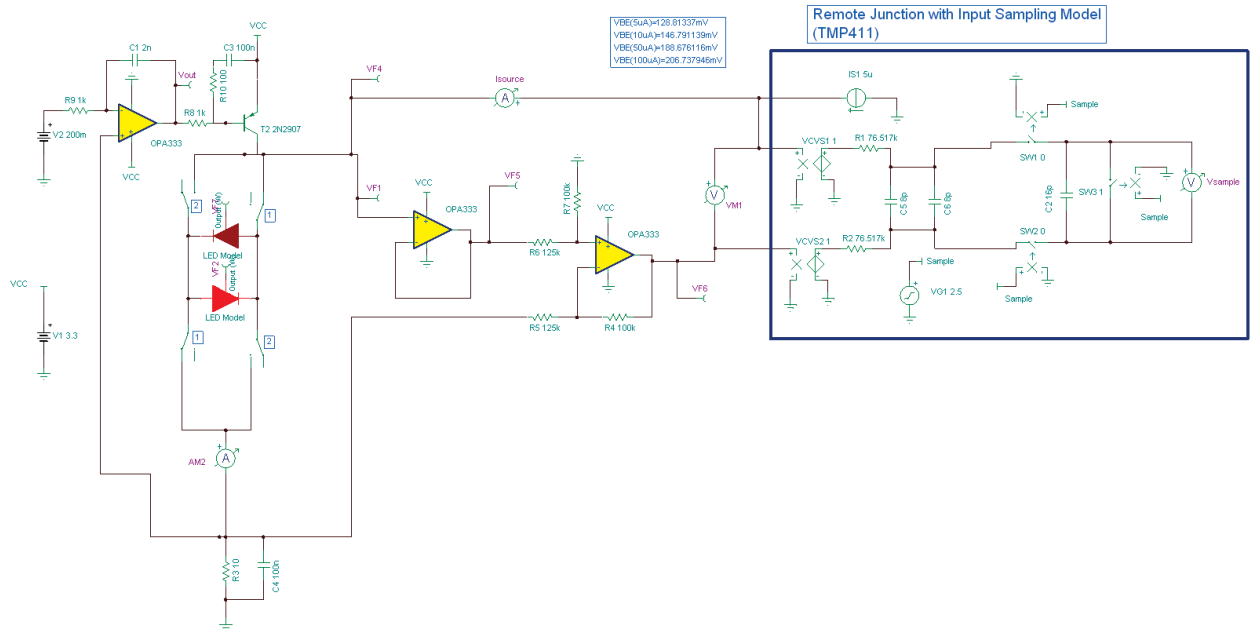

Figure 21: LED driver circuit with temperature sensor

5.2.4 Transimpedance Amplifier

The purpose of the analog frontend was to measure electrical signals from the photodetector and provide an amplified, low-noise, accurate signal to the microcontroller. A block diagram showing the analog frontend and the adjoining components is shown in Figure 22. In accordance with the functional requirements, the design needed to provide the microcontroller with a sufficiently accurate signal such that O_2 levels could be calculated within ±2% of the actual value. In addition, it needed to cleanly amplify signals of varying amplitude. It was expected that current levels from the photodiode would range from 10nA to 10µA. In order to meet the 12+ hour battery life requirement, the analog frontend needed to be designed for minimal power dissipation. In order to meet the constraints placed on the design, parts operating on low power and low voltage in addition to having a small form factor were selected. Furthermore, the number of active parts was limited to reduce power use.

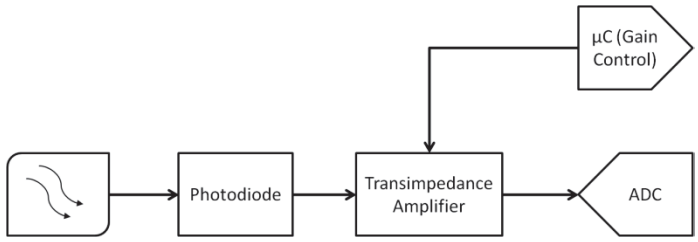

Figure 22: Block diagram of analog frontend and adjoining components

There are four methods of electrical signal amplification, each with advantages and disadvantages.

- Voltage-to-voltage: Easy to implement, but the voltage obtained from photodiode signal would be very small and thus difficult to accurately amplify.
- Current-to-current: Would directly amplify the photodiode current, but the analog frontend would connect to an analog to digital converter (ADC), which measures voltage not current. To translate the signal into a voltage, the current would need to flow through a passive or active element which would increase power consumption.
- Voltage-to-current: Combines the shortcomings of both prior methods.
- Current-to-voltage: Makes use of the current output by the photodiode and amplifies it as a voltage that an ADC could read.

The optimal choice was a current-to-voltage amplifier, also called a 'transimpedance amplifier'. In its simplest form, the transimpedance amplifier consists of an op-amp core and a resistive feedback loop (see Figure 23). The voltage at the output of the amplifier is the product of the photodiode current, I_{ph}, and the feedback resistor, R_{fb}. However, to properly model the amplifier, the capacitance of the photodiode, C_{ph}, needed to be taken into account. The photodiode capacitance introduced a pole into the feedback factor that de-stabilized the amplifier without a compensation capacitor, C_{fb}. The compensated amplifier design can be seen in Figure 23 as well.

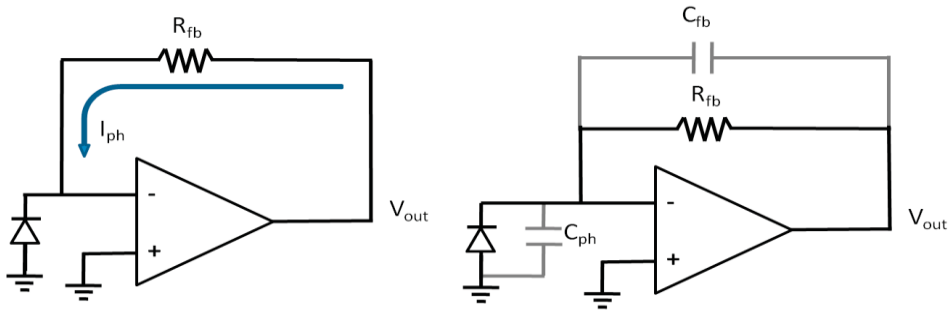

Figure 23: (Left) Simple transimpedance amplifier. (Right) Compensated transimpedance amplifier

The stability analysis was performed by analyzing the open-loop gain (A_{OL}) of the op-amp and the gain response of the feedback network (feedback factor or β). To ensure stability, the product of the open-loop gain and the closed-loop gain ($A_{OL}\beta$) could undergo an 180° phase shift by the time unity gain was reached. This was illustrated by using a log-graph of A_{OL} and 1/β (see Figure 24). The point at which the two lines intersect is unity gain. To preserve stability, the 'rate of closure', or rate of $A_{OL}\beta$ change at the intersection, cannot be greater than or equal to -40 dB/decade. This is because -40 dB/decade implies a 180° phase shift (under the assumption that the poles are at least a decade apart).

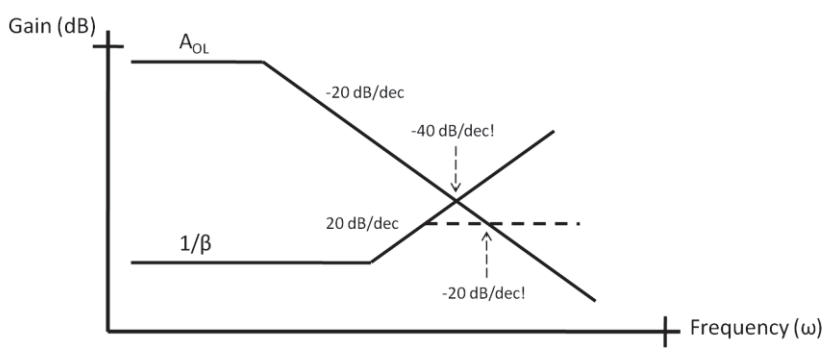

Figure 24: Gain curves for A_{OL} and 1/β

To mitigate the instability, a compensation capacitor C_{fb}, was added to the feedback network (see Figure 25). This capacitor inserted a zero into β to roll-off the gain before the intersection with the A_{OL} curve, thus reducing the rate of closure to -20 dB/decade. This can be seen in Figure 24 as the dashed line. The precise location of the roll-off affected the phase margin and bandwidth of the system. To ensure that there was no ringing in the system, C_{fb} was chosen to give at least a 60° phase margin. To reduce high frequency noise, an RC low-pass filter with a cut-off frequency equal to $A_{OL}\beta$ unity gain was also added to the amplifier.

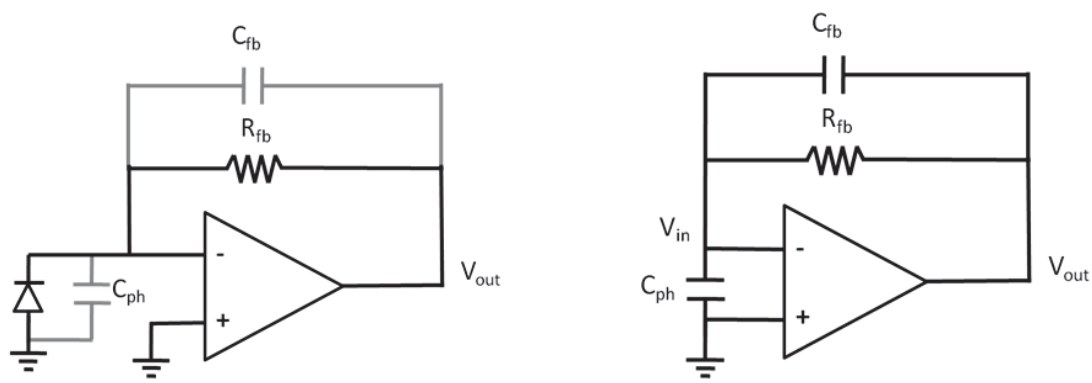

Figure 25: (Left) Transimpedance amplifier. (Right) Small signal transimpedance amplifier

Equations 3-6 show the method to solve for the feedback factor, β, which is equal to V_{in}/V_{out},

$$\frac{V_{out}-V_{in}}{\left(\frac{R_{fb}}{1+sR_{fb}C_{fb}}\right)}=\frac{V_{in}}{1/sC_{ph}} \tag{3}$$

$$\frac{V_{out}}{\left(\frac{R_{fb}}{1+sR_{fb}C_{fb}}\right)}=\frac{V_{in}}{1/sC_{ph}}+\frac{V_{in}}{\left(\frac{R_{fb}}{1+sR_{fb}C_{fb}}\right)} \tag{4}$$

$$\frac{V_{out}}{V_{in}}=\frac{sC_{ph}R_{fb}}{1+sR_{fb}C_{fb}}+1 \tag{5}$$

$$\frac{V_{in}}{V_{out}}=\frac{sR_{fb}C_{fb}}{1+sR_{fb}\left(C_{fb}+C_{ph}\right)} \tag{6}$$

After analyzing the β equation (Eq. 6), it was evident that the sum of the photodiode and feedback capacitance created a pole in the feedback loop. The feedback capacitor created a zero which was used to roll-off the feedback gain and ensure stability.

Meeting the requirement of ±2% accuracy of SpO_2 saturation was of paramount, as a person could die because as the result of an inaccurate reading. To ensure an accurate measurement, noise had to be taken into account and the transimpedance amplifier had to be designed to restrict noise. A 100% oxygen saturation level corresponds to a 0.5 ratio of IR to Red light intensity and an 82% level corresponds to a 1.0 ratio. Assuming linearity, a 2% change is equivalent to a 0.056 change in the ratio of

light intensities. In the worst case, the noise on each light signal is 180° out of phase. Equations 7-10 below outline the method used to find the maximum SNR needed to maintain an accurate measurement.

$$0.5 + 0.056 = \frac{v_{signal} + v_{noise}}{2v_{signal} - v_{noise}} \tag{7}$$

$$\left(2v_{signal} - v_{noise}\right)0.556 = \left(v_{signal} + v_{noise}\right) \tag{8}$$

$$0.112v_{signal} = 1.556v_{noise} \tag{9}$$

$$\frac{v_{signal}}{v_{noise}} = SNR \cong 13.89 \tag{10}$$

As seen by Eq. 10, the maximum calculated SNR that could still result in a ±2% accuracy was 13.89. Taking into account the quantization noise of the DAC, we then calculated the minimum number of required bits to achieve the maximum allowable SNR,

$$SNR = 13.89 \cong 22.85dB \tag{11}$$

$$SNR = 6N + 1.76dB \tag{12}$$

$$22.85dB = 6N + 1.76dB \tag{13}$$

$$N \cong 3.52 \tag{14}$$

$$\text{Min. Bits Required} = 2^N \cong 11.44 \tag{15}$$

Rounding to the closest integer,

$$\text{Min. Bits Required} = 12 \tag{16}$$

In terms of transimpedance core op-amp selection, noise, capacitance, open-loop bandwidth, power, and output swing were considered. The op-amp used in the transimpedance core needed to have low voltage and current noise. In addition, the input capacitance of the amplifier had to be small (on the order of 1 pF or smaller) as the input capacitance reduced the bandwidth of the transimpedance amplifier. This was due to the input capacitance being added to the capacitance of the photodiode. A

large open-loop bandwidth was preferable, but since large bandwidth amplifiers tend to use more power, the power dissipation of the amplifier had to be carefully considered. The higher the bandwidth, the more accurate the amplified signal. That is, if a square pulse were the input, a high bandwidth op-amp would accurately output an amplified square pulse. A low bandwidth amplifier may have output a signal closer to a saw tooth shape. Because the amplifier was required to operate between 3.3 V and 0 V, an op-amp capable of rail-to-rail operation was desirable. Finally, the input current of the op-amp was required to be small. Even a small input current would induce a significant DC offset on the output. Only the AC component of the photodiode was of interest, but large DC offsets could push the signal to the rails. To mitigate this risk, an FET-based op-amp was selected.

There were three main candidates for the transimpedance amplifier stage: the OPA363, OPA381, and OPA376. Ultimately, we selected the OPA376 because of its superior noise and input current characteristics. The OPA376 uses 150µA more quiescent current than the OPA363, but it was deemed an acceptable trade-off due to the better performance.

Initially, a LED pulse width of 50µs was chosen. It was also desired that the pulse settle over a period of 12 time constants. The number of time constants chosen affects the required bandwidth, required gain, and maximum number of bits of resolution (more time constants corresponds to more resolution).

The required open-loop bandwidth was calculated as follows,

$$f_{clBW} = \frac{\left(0.35 + \frac{\tau_{num}}{2\pi}\right)}{t_{sample}} = \frac{2.26}{50\mu\text{s}} \cong 45.2kHz \tag{17}$$

$$f_{clBW\max} = 1.25 f_{clBW} \tag{18}$$

$$f_{opBW} = 10 f_{clBW\max} \cong 565\text{kHz} \tag{19}$$

The OPA376 met the bandwidth requirement calculated in Eq. 19.

In order to limit the noise, several RC low-pass filters were implemented to roll-off the noise gain from the feedback loop. To decrease the effect of noise in the system, the closed-loop bandwidth was limited. Because of this, the LED pulse width had to be increased to 500µs. The new closed-loop bandwidth calculation is shown in Eq. 20.

$$f_{clBW} = \frac{\left(0.35 + \frac{\tau_{num}}{2\pi}\right)}{t_{sample}} = \frac{2.26}{500\mu s} \cong 4.52kHz \tag{20}$$

To limit the noise in the system, low-pass filters at twice the closed-loop bandwidth, 10kHz, were placed in different paths in the amplifier. The 3dB cutoff frequencies for the low-pass filters were placed at twice the closed-loop bandwidth to avoid shrinking the closed-loop bandwidth unnecessarily. As can be seen in Figure 28, low-pass filters were placed at the output of each amplifier stage as well as inside the feedback loop of each stage to limit the noise gain. The resistor values at the outputs of the amplifiers had to be at least 5-10 times greater than the output impedance of the amplifiers at 10kHz. Thusly, a 1kΩ resistor was chosen for the low-pass filter at the output of the OPA376 and a 10kΩ resistor was used for the low-pass filter at the output of the OPA333.

The feedback capacitor and resistor needed to be low noise. To ensure low voltage noise from the capacitor, a low Equivalent Series Resistance (ESR) capacitor was chosen. To reduce the noise from the feedback resistor, a high power, 0805 metal-film resistor was chosen (larger area resistors have lower noise). In order to mitigate the large resistance and small capacitance requirements of the feedback network, a 'tee' network was considered, as in Figure 26. A tee network significantly increases equivalent resistance or decreases equivalent capacitance values so that more reasonably-valued components can be used. However, the consequence of a tee network was increased noise, which ultimately rendered it impractical.

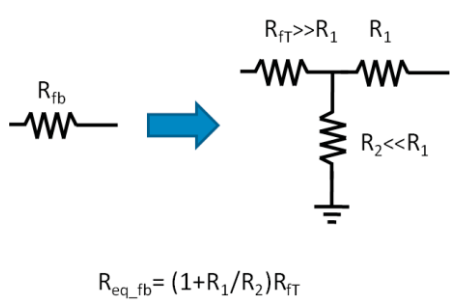

Figure 26: Resistive tee network

To increase the bandwidth of the amplifier, the photodiode could be operated in photoconductive mode. That is, a large voltage is dropped across the photodiode to place it in reverse bias. This increases the width of the diode depletion region, thus decreasing the capacitance. The reduction in capacitance pushes the pole in the feedback factor to a higher frequency, which increases the bandwidth. In addition, the reverse bias increases the sensitivity of the photodiode. However, this increase in sensitivity increases noise, and a DC current, known as 'dark current', will continually flow. The alternative was photovoltaic operation of the photodiode. In this mode, no voltage is dropped across the photodiode. The capacitance of the photodiode is greater, but it does not suffer from the noise and dark current present in photoconductive operation. Using a technique known as 'bootstrapping', the effective capacitance of the photodiode can be reduced by several orders of magnitude while remaining in photovoltaic mode. Bootstrapping requires a voltage buffer to be placed around the photodiode. This buffer has similar requirements to the transimpedance core op-amp, it must have low noise, negligible input current, and small input capacitance. The bootstrapping configuration is shown in Figure 27.

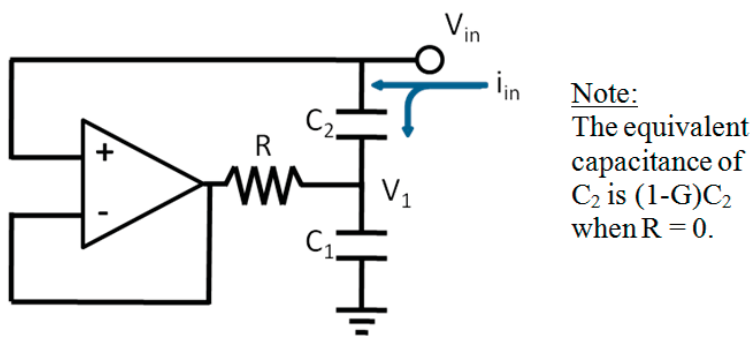

Figure 27: Bootstrapping configuration

The current into V_{in} is given by Eq. 21. Performing KCL at the node V_1, we get Eq. 22,

$$i_{in} = \frac{V_{in} - V_1}{1/sC_1} \tag{21}$$

$$\frac{V_1}{1/sC_1} = \frac{V_{in} - V_1}{1/sC_1} + \frac{GV_{in} - V_1}{R} \tag{22}$$

Where G is the buffer gain (G≈1). Solving for V_1 from Eq. 22,

$$sC_1V_1 + sC_2V_1 + \frac{V_1}{R} = sC_2V_{in} + \frac{G}{R}V_{in} \tag{23}$$

$$V_1 = \frac{V_{in}\left[sC_2 + \frac{G}{R}\right]}{sC_1 + sC_2 + \frac{1}{R}} = \frac{V_{in}\left[sRC_2 + G\right]}{sR\left(C_1 + C_2\right)+1} \tag{24}$$

Solving for the equivalent impedance of C_2 (photodiode), V_{in}/i_{in},

$$i_{in} = \frac{V_{in}\left[1 - \frac{sRC_2 + G}{sR\left(C_1 + C_2\right)+1}\right]}{1/sC_2} \tag{25}$$

$$i_{in} = V_{in}\left[sC_2 - \frac{s^2RC_2{}^2 + sGC_2}{sR\left(C_1 + C_2\right)+1}\right] \tag{26}$$

$$\frac{V_{in}}{i_{in}} = \left[\frac{s^2RC_2\left(C_1 + C_2\right) + sC_2 - s^2RC_2{}^2 + sGC_2}{sR\left(C_1 + C_2\right)+1}\right]^{-1} \tag{27}$$

$$\frac{V_{in}}{i_{in}} = \left[\frac{sR\left(C_1 + C_2\right)+1}{s^2RC_1C_2 + sC_2 - sGC_2}\right] \tag{28}$$

Eq. 28 is the equivalent impedance looking into node V_{in}. For a small R, large C_1, and a buffer gain close to unity gain, the equivalent capacitance of C_2 becomes very small.

Ultimately, photovoltaic operation was chosen due to the lower noise and lower power dissipation of the photodiode. Bootstrapping was also not used as the capacitance of the chosen photodiode was approximately 20pF. At such a low capacitance value, the closed-loop bandwidth was not limited by the photodiode and bootstrapping was unnecessary. The final transimpedance amplifier design used is shown in Figure 28.

There are several adjustable features of the transimpedance amplifier. Firstly, to mitigate a high DC offset on the signal, the microcontroller DAC can apply a voltage to the V_{off} terminal, seen in Figure 28. Increasing values of V_{off} will shift the DC level of the signal towards ground. There are two feedback

loops in the gain stage (the amplifier on the right in Figure 28); the microcontroller controls which of the two feedback paths are used. One has a gain of 2, the other a gain of 10, and both have 3dB points at 10kHz.

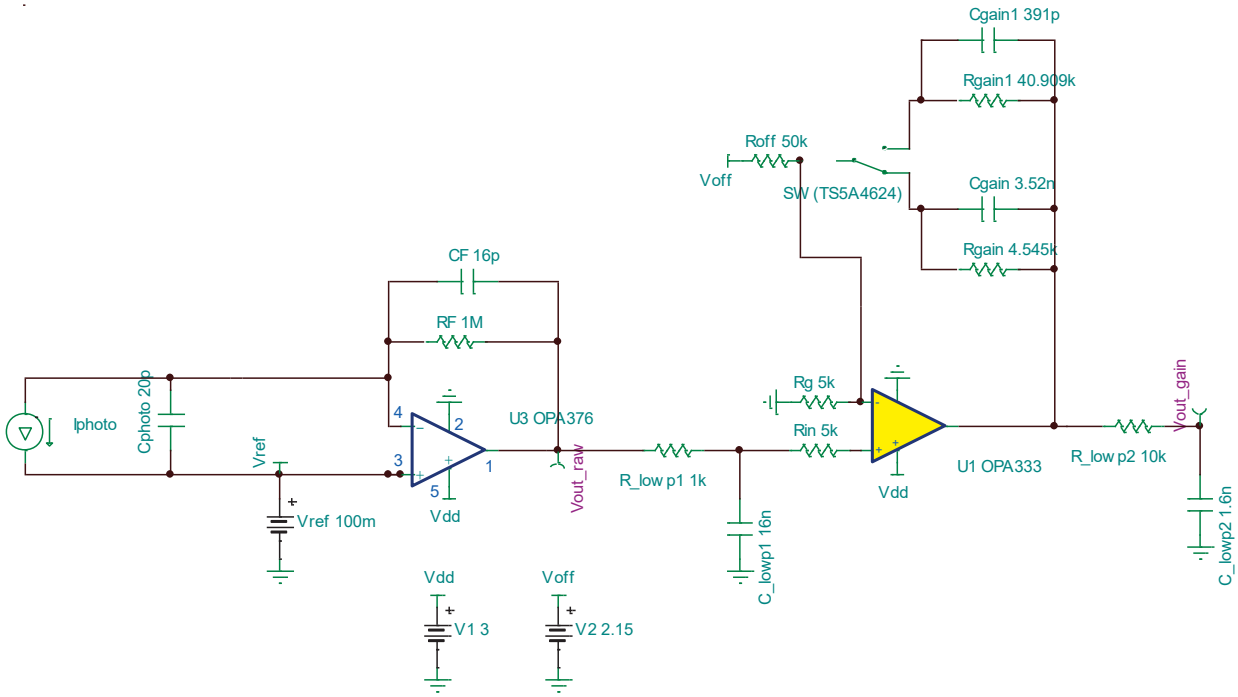

Figure 28: TINA circuit layout of the transimpedance amplifier

TINA simulations were performed on the transimpedance amplifier circuit to ensure its operation before breadboarding. The circuit was modeled using a 20 pF capacitor and current source as a photodiode. There was a 100 mV DC bias applied to the transimpedance core op-amp to avoid dipping below the minimum input voltage of the OPA376.

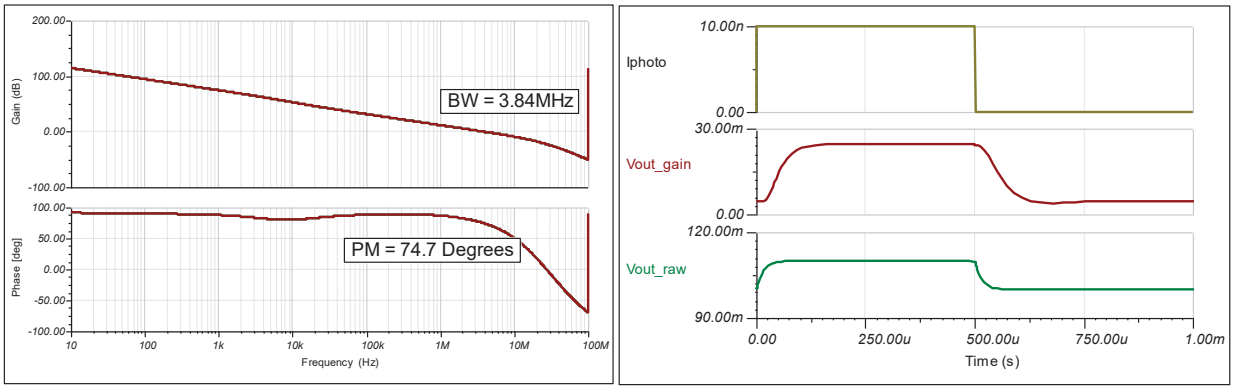

Figure 29: (Left) Frequency response of transimpedance amplifier. (Right) Transient response to 10nA, 500µs pulse

From Figure 29, the phase margin of the amplifier was 74.7° with a bandwidth of approximately 3.84 MHz. The DC gain was approximately 125 dB. The output voltage of the amplifier, in response to a current pulse, is shown is also shown in the figure (at right). The output had no overshoot, as was expected, with a phase margin larger than 60°.

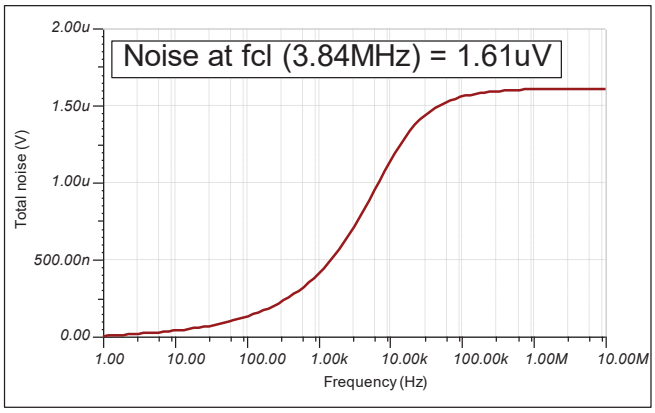

Figure 30: Noise analysis of transimpedance amplifier

Figure 30 shows a noise analysis performed on the transimpedance amplifier using the TINA software. Based on the noise at the open-loop bandwidth, the SNR of the transimpedance amplifier was calculated as follow,

$$v_{signal} = 10nA \cdot 1M\Omega \cdot 2\,{}^{V}\!/_{V} = 0.02V \tag{29}$$

$$SNR = \frac{v_{signal}}{v_{noise}} = \frac{0.02V}{1.61\mu V} \cong 12422 \tag{30}$$

Thus, the maximum number of bits for the resolution of the transimpedance amplifier was,

$$n = \frac{\log(1 + V_{DD} \cdot SNR)}{\log(2)} \cong 15.19 \tag{31}$$

Rounding to the lowest integer,

$$n = 15 \tag{32}$$

This result satisfied the requirements necessary for achieving ±2% oxygen saturation accuracy.

5.2.5 Digital Interface

The purpose of the digital interface is to control all of the analog circuitry. This is done by collecting and transmitting the data from the analog circuitry to the user interface. The digital interface consists of two MSP430 microcontrollers, an analog to digital converter, two wireless transceivers, and a USB interface device. A microcontroller unit (MCU) was needed that would be capable of communicating with all of the peripherals including the ADC and temperature sensor, which both use an I^2C interface, and the RF transceiver which uses the SPI protocol. The controller also needed several timers to regulate the pulses for the LED driver, as well as two onboard DACs to set the brightness of the LED driver and to regulate the gain of the gain stage. To accommodate all of these requirements the MSP430FG477 MCU was chosen as it had all of the necessary components and its size was small enough to fit well with the other components.

The first digital to analog converter (DAC0) was used to control the brightness level of the red and infrared LEDs. This brightness varied depending on the voltage coming out of the analog frontend. In order to get both LEDs to flash alternately, a timer was set on the microcontroller to interrupt every 10ms, giving a period of 100Hz. Each time this event was triggered a pin connected to the switch portion of the LED driver toggled. A second interrupt would then occur 50us after the first interrupt toggled the pin, creating a total pulse width of 50us. During this time, DAC0 would send out a voltage dependent on which LED was being toggled. In order to sample the voltage coming out of the transimpedance amplifier, a read of the 12-bit ADC would also happen during this 50us pulse. The second digital to analog converter (DAC1) was used to set the gain for the gain stage. There were two bias voltages needed for this stage in order to output a stable signal.

The analog to digital converter that was chosen was the ADS1015 12-bit ADC. This was chosen both because it came highly recommended by our sponsor and it was easy to communicate with. In order to configure the ADC, correct commands must be sent via I^2C. The ADS1015 needs an address command (0x48 for the chip used) followed by a write to the pointer register, which selects the register that needs to be configured (see Table 3). Once this occurs, the next two bytes are used to set the configuration setting (see Table 4).

Table 3: Bits 1 and 0 of the pointing register which determine where the next read/write will occur

BIT 1	BIT 0	REGISTER
0	0	Conversion register
0	1	Config register
1	0	Lo_thresh register
1	1	Hi_thresh register

Table 4: Both bytes of the configuration register to be written to

BIT	15	14	13	12	11	10	9	8
NAME	OS	MUX2	MUX1	MUX0	PGA2	PGA1	PGA0	MODE
BIT	7	6	5	4	3	2	1	0
NAME	DR2	DR1	DR0	COMP_MODE	COMP_POL	COMP_LAT	COMP_QUE1	COMP_QUE0

For the purposes of this project, the following registers were written to in order to correctly configure the unit for conversions.

1. Pointer Register 0x01: Selects the configuration register.
2. Configuration Register 0x42: Selects continuous mode, FSR voltage of +/- 4.096V, and selects AIN0 as AINp and ground as AINn.
3. Configuration Register 0x83: Selects 1600 samples per second and disables the comparator.
4. Pointer Register 0x00: Selects the conversion register.

From here, a simple read command, which consisted of sending the address with the read bit set, followed by two bytes of clock signal was used to read the data from the conversion register. This data was then entered into Eq. 33 to get the voltage level.

$$V_{ADC} = \frac{ADC_{code} * 4.096}{4096} \tag{33}$$

The MCU also controlled the temperature sensor using the I^2C interface with the same method described for the ADC. Data was written to the temperature sensor to set the temperature coefficients of the two LEDs, which were subsequently read. This occurred once every three seconds to minimize power consumption. In the case that the LEDs reached a threshold, DAC0 then limited their brightness until they reached a safe temperature.

The EZ430-RF2500 RF module was chosen for the wireless interface. This selection was made because the protocol was already written and because of its convenient compact size. The code was easily transferred from the MSP430F2272 to the MSP430FG477 and implemented on the board that we prototyped. The actual RF transceiver implemented was TI's CC2500, which uses a serial peripheral interface (SPI) protocol to communicate with the microcontroller. Combining this with TI's SimpliciTI wireless communication protocol allowed successful transmissions of data from the microcontroller to the EZ430-RF2500 USB stick. The only data that was actually sent from the digital interface to the user interface was the voltage level and its corresponding LED, which was sent over in a 2-bit array of data.

5.2.6 User Interface

The purpose of the user interface was to display the recorded data from the microcontroller via wireless interface. It also needed to able to sound an alarm when a low oxygen level was reached. These two functional requirements had to be met for a successful design of the user interface. The alert signal was constrained by an audible level around 80dB so that it could be easily heard and responded to but not as loud as to damage a person's hearing.

TI also had a separate requirement that the user interface be implemented for an iPhone. This was attainable because Apple makes a software development kit (SDK) available for the public to develop software for the iPhone OS. The iPhone OS is the operating system that the iPhone and iPod Touch use for operation. Since an iPhone was more expensive than an iPod Touch and had features that the project did not require, the final device was used with the pulse oximeter prototype was an iPod Touch. The iPod Touch had Bluetooth and WiFi capabilities that could be used for wireless communication. The Bluetooth was limited by the SDK to peer-to-peer communication so we had to use the WiFi to connect to the intermediary pass-through device. It also had a speaker to accommodate the alert signal, a file system allow the saving of files, an LCD to display the GUI, and a development framework allowing access to these features.

The SDK used Objective C as its primary language along with C, Java, and some C++ being able to be used as well. The SDK provided several tools to help in the application development process. These tools were Xcode, Interface Builder, and Instruments. Xcode is an integrated development environment (IDE) for writing code for Apple's products. Interface Builder is a tool allowing the GUI to be created graphically rather than programmatically (writing code). Instruments is a utility that gave a plethora of

vitals on the application in the debug process which included a leak detector and memory usage. Apple provided these tools to developers to streamline the process of creating software for their products.

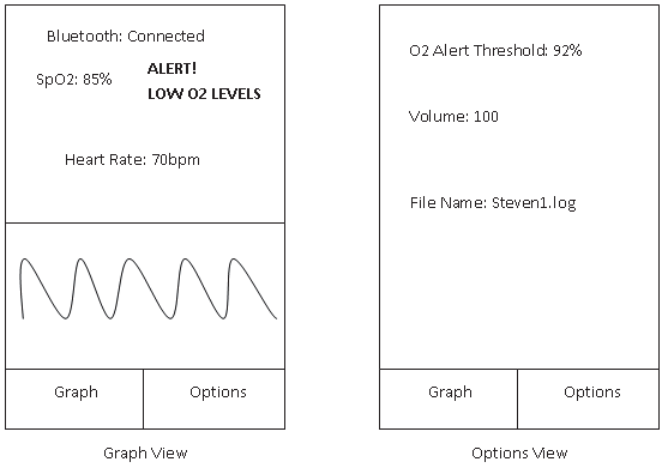

Figure 31: Design template for user interface featuring 2 main screens

Figure 31 shows a preliminary layout of the GUI that was used as a design template. Figure 32 shows the completed GUI for the user interface with test data visible.

Figure 32: Final user interface GUI implemented on iPod Touch

The underlying program flow for the user interface is shown below in Figure 33. The program flow shows how the user interface operates. It manages the WiFi connection, listens for data, verifies the data, updates the GUI, and manages the alert sound.

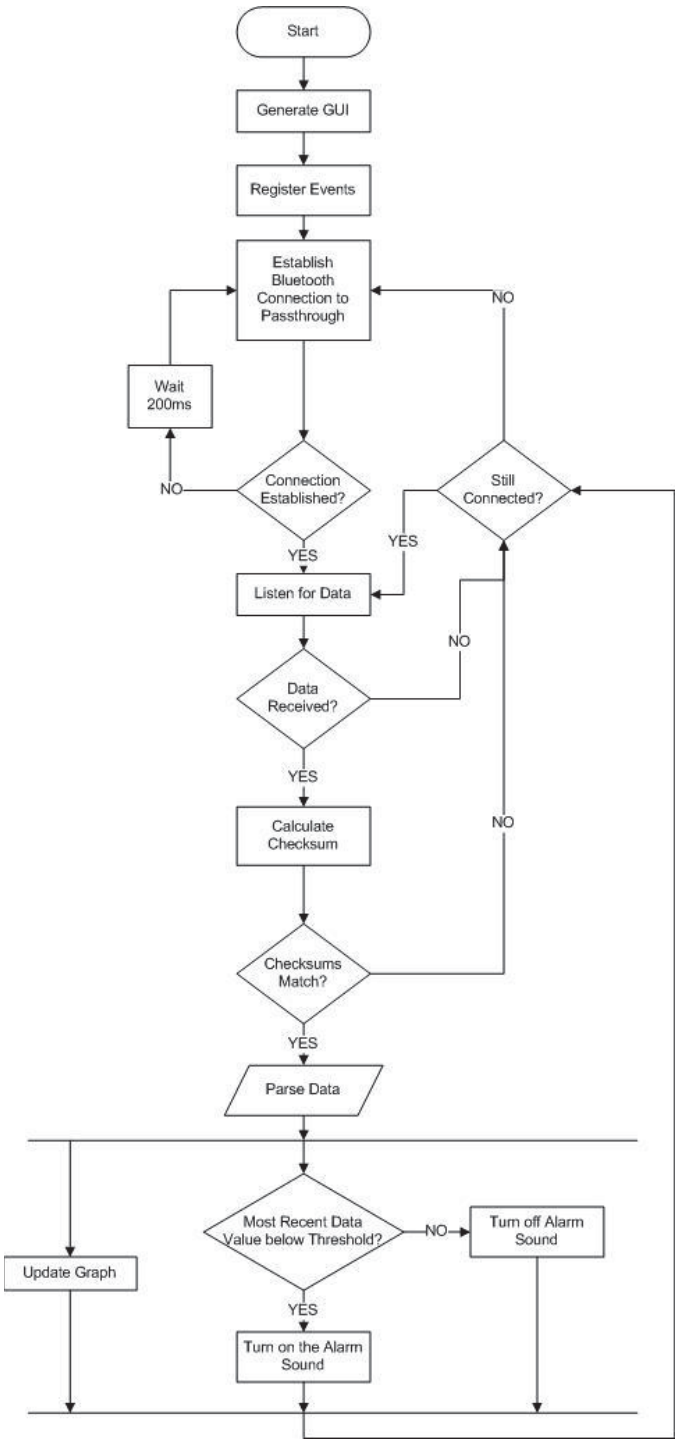

Figure 33: User interface program flow

The user interface used a few examples GUIs to help with development. The first was sample code from Apple that was used to develop the WiFi and FTP functionality. Specifically, the sample code named *SimpleNetworkStreams* [7] was used for the WiFi and *SimpleFTPSample* [6] was used for the FTP connection. They allowed for functioning connections that could then be modified to what was needed for the user interface. The plotting software used was from an open source plotting framework called *Core Plot* [2]. *Core Plot* simplified the graphing function of the user interface. It was able to periodically update the graph to the new data from the WiFi. This allowed the data to be viewed in real time.

For the calculations of oxygen saturation and heart rate, a peak detection algorithm was used in the time domain to find the peaks and troughs. This algorithm is based on Matlab code from Eli Billauer on his website [1]. This allowed the minimum and maximum of each pulse and time between pulses to be used in several calculations. The heart rate was found to be sixty divided by the time between the last two pulses. This was then compared to the last calculated heart rate to see if it was a possible value since the peaks and troughs found contained the data from the dicrotic notch and noise, which would give incorrect saturation and heart rate data. Since the peak of the pulsatile wave and dicrotic notch could be used to calculate the heart rate, it would report a substantially higher heart rate than the actual heart rate. To eliminate this issue, the program rejects the last peak or trough and keeps the last heart rate if the calculated heart rate is incorrect. Then the oxygen saturation is calculated using the data where the dicrotic notch data points were removed. This method allowed for the most accurate readings.

A fast Fourier transform (FFT) was going to be used to calculate the AC and DC components of the pulsatile waveform and the heart rate but it would have caused several problems. First, a sample size of 2048 data points at a sampling rate of 34Hz was required to achieve a heart rate resolution of 1 beat per minute. This would have caused the iPod Touch to become sluggish from the calculations since the FFT algorithm is $O(n*\log_2(n))$ or that it would have taken $256*\log_2(2048) = 2816$ loop iterations to obtain the information that was needed. Second, a sample size of 2048 data points would have obscured the actual changes in heart rate. Lastly, the FFT algorithm could not handle transients correctly. For example, if a person had a rising saturation, the pulsatile waveform would look like the steady state waveform that had been rotated toward in an increasing manner. These transient conditions caused the FFT to produce incorrect values. Overall, the FFT could not handle transient conditions in heart rate or saturation. These problems could be resolved with a smaller sample size such as 64 points but then the heart rate would be incorrect by more than 15 beats per minute which was unacceptable. In the peak detection scheme,

the heart rate was extremely accurate and the oxygen saturation calculations could be corrected using linear interpolation [8]. The FFT was not used because of these problems.

6 System Build

The completion of the design process led to the development of a robust testing procedure designed to ensure that the final pulse oximeter operated correctly and met the functional requirements laid out by the project sponsor. The testing process was implemented in two stages: the first stage was designed to test the individual subsystems of the pulse oximeter, while the second tested the final, assembled pulse oximeter as a whole.

6.1 Subsystem Testing

Prior to any integration of the individual subsystems, each was tested independently as a stand-alone system in order to validate basic functionality, as well as eliminate as many potential compatibility issues as possible. The subsystem testing was divided into two primary stages: breadboard testing and PCB testing. The breadboard testing phase was the initial mockup for each of the electronic circuits using discrete components, in order to establish baseline values for the electrical parameters of interest. The shortcomings of breadboard testing lie in the large amount of capacitance inherent to breadboard designs. This capacitance has the potential to induce additional noise into the measured signals, which was particularly prevalent in the small signals seen at the transimpedance amplifier input.

Once basic functionality had been established through breadboard testing, a prototype PCB was created that encompassed the transimpedance amplifier, microcontroller, and LED driver circuits. Further testing revealed that the PCB circuits were much less prone to noise saturation than their breadboard counterparts, making for more accurate signal acquisition. The information in Table 5 outlines the tests performed on the individual subsystems and defines the required condition, testing procedure, metric, and expected as well as final results of the testing. Table 6 details the equipment used throughout the testing process.

Table 5: Subsystem testing procedures and results

Subsystem	Requirement	Measurement Procedure	Metric	Expected Result	Actual Result	Pass/ Fail
LED Driver	Provide a linear variable output current	Measure the output current as input voltage changes	Amps	0-30mA linear current	0-29.6mA linear current	✓
	Provide a square wave output current at 1kHz	Measure output current with an oscilloscope while switch is in circuit	Amps	Square wave with rise/fall times of the current level at 1kHz	More of a triangle wave at current level at 1kHz (Usable signal)	✓
	Have correct LED function with known Nellcor oximeter sensor	Verify that both Red and IR LEDs pulse at proper rate and sequence	Visual Pulse	Both LEDs pulsed opposite each other at 1kHz	LEDs pulse alternately, similar to commercially available units	✓
LED Driver & Temp Sensor	Circuit produces desired voltage across LEDs	Measure the V_{be} across the LED with multimeter	Volts	Voltage across LEDs between 0-1.1V	1.9V voltage drop across both LEDs	✓
User Interface	Transmit data via WiFi	Transmit text from computer to iPod Touch	Visual	Correct message displays on screen	Correct message displayed on screen	✓
	Plays sound	Run code to produce sound	Aural	Sound clip is heard	Sound played correctly	✓
	Parse and graph data	Observe the graph	Visual	Data graphed correctly	Data graphed correctly	✓
	Data translated	Input data to RF and receive output on WiFi	Visual	Data received correctly	Data received correctly	✓
	GUI functions correctly	Use the program on iPod Touch to find faults/bugs	Visual	No faults/bugs	No faults/bugs found	✓
	Live data streaming	Observe the graph	Visual	Graph updates correctly	Graph updates in real time	✓
	Alert threshold functions correctly	Observe when levels go below threshold	Aural/ Visual	Alert sounds when level falls below threshold	Alert sounds at low levels	✓
	Data logging	Inspect datalog generated from data received	Visual	Data is present and well formed	Data is present and well formed	✓
Digital Hardware	Communicate between microcontroller and ADC	Verify I2C signal lines	Volts	9 cycle clock and data	Stable clock	✓
Transimpedance Amplifier	Amplifier stable with photodiode on input	Apply step input and observe stability of output	Volts	Saturated or unsaturated output	Stable output for photodiode with large junction capacitance	✓
	Amplify 10nA to 1uA photodiode signal	Use OxSim and Nellcor sensor to inject current	Volts	Amplified square wave voltage with DC offset	Square wave output with high frequency noise; heart beat detected	✓
	Output square wave settles fast enough for ADC to sample peak signal	Measure settling time	Time	Settles quickly (should not see much overshoot with PM=80°)	With 50µs pulses, output wave settles in a sufficient amount of time	✓

Table 6: Testing equipment

Description	Manufacturer	Part Number
Oscilloscope	Tektronics	TDS2014B
Function Generator	Hewlett-Packard	33120A
Triple DC Power Supply	Agilent	E3631A
Current Source	Yokogawa	GS610
Digital Multimeter	Agilent	34401A
Voltage Source	Data Precision	8200

6.2 Subsystem Integration

Following the independent subsystem testing, the next step was to combine the subsystems into a single, functioning pulse oximeter. The initial input is taken at the photodiode; the output current from the photodiode is proportional to the amount of light absorbed from the LEDs after passing through the user's earlobe or fingertip. The LED driver circuit is responsible for receiving commands from the microcontroller in order to pulse light appropriately. The photodiode output current is received by the transimpedance amplifier, converted to a voltage, and sent to the microcontroller. The microcontroller in turn transmits the signals via WiFi to the user interface, where the data is sorted and expressed as a percentage of oxygen concentration.

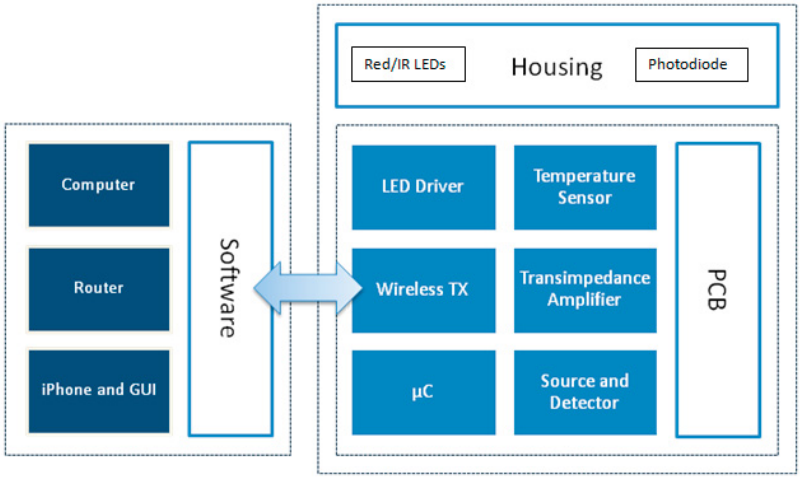

Figure 34: Full system flowchart

Physically, the subsystems are integrated in three major parts: the components contained within the physical housing, the components contained within the sensor housing, and the components of the user interface. The flowchart presented in Figure 34 indicates how the various subsystems interface with one

another. The microcontroller, LED driver, and wireless transmitter circuits are located on a single PCB, located within the main housing, which mounts to the arm of the wearer. The LEDs, photodiode, and transimpedance amplifier are located in the sensor housing, which clamps around the ear of the wearer. The sensor housing and main housing are connected via a wire and an FPC connector that is accepted by the main housing. The remaining portions of the pulse oximeter are implemented in the user interface itself, within the GUI application that is displayed on the iPod. The user interface is where data transmitted over WiFi from the microcontroller is received and displayed. The PCB layout for the main board containing the microcontroller, LED driver, and wireless transmitter is shown in Figure 35. The dimensions of the final board were 2.969" by 0.881".

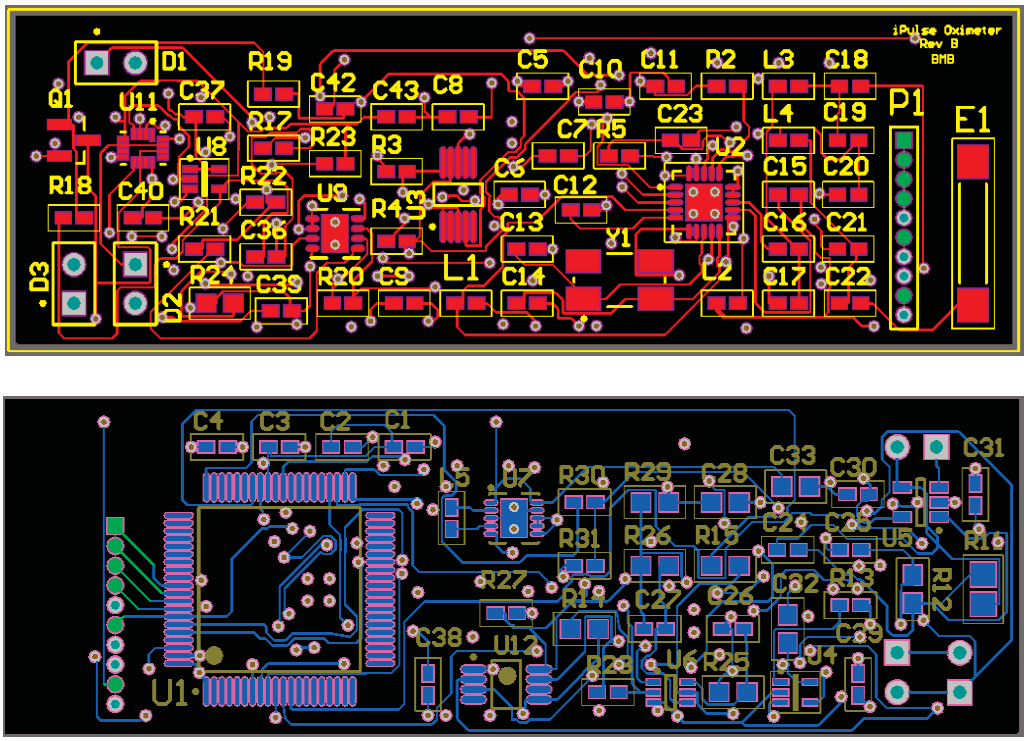

Figure 35: PCB layout for main housing board

7 System Testing

Upon completion of the subsystem interfacing, the final step in the testing procedure was to verify that the completed pulse oximeter met all of the specified functional requirements. Table 7 outlines the tests performed on the pulse oximeter in order to verify full system functionality and more details on the individual testing procedures and results are presented in the following sections.

Table 7: Overall system testing procedure and results

Requirement	Measurement Procedure	Metric	Expected Result	Actual Result	Pass/ Fail
Accuracy – accurate to within ±2% of actual blood oxygen concentration	Compare 0_2 concentration values from remote pulse oximeter with those of Massimo oximeter	Oxygen saturation (%)	±2% difference from Massimo oximeter readings		?
Perceptible Alert Signal - audible alert during low oxygen conditions	Generate a simulated low oxygen signal in order to trigger alert	Decibels	80dB alert signal triggered at adjustable low oxygen level	65dB at 1m ~80dB at ~0.5m	✓
Battery Life - remain functional for desired time on battery power	Run oximeter continuously until electronic components shut off due to insufficient power from battery	Time (Hours)	Oximeter will be able to run continuously for 12 hours or longer	~2 hours continuous use	✓
Transmission Distance - wirelessly send data over the required distance	Gradually separate oximeter from user interface until data is no longer transferred	Distance (m)	Transmit data no less than 25m	~35m	✓
Data Logging – ability to continuously monitor data for specified time period	Run oximeter over course of one night, observe file size, multiply by seven	Time (Weeks)	At least 1 week worth of data logged from continuous monitoring	~11MB/week (iPhone has 8GB of capacity)	✓
Shock Resistance – system must remain functional after 2m fall	Model housing and components in SolidWorks and conduct FEA analysis to predict performance	Stress (N/m^2)	Oximeter will maintain full functionality after fall	SolidWorks verification of maximum stress of ~$400kN/m^2$	✓
Water Resistance – resistant to a depth of 3m	Submerge in water for period of 30 seconds	Distance (m)	Oximeter will maintain full functionality after water submersion	Not performed due to time constraints	✗

7.1 Housing Testing

The testing that was done for the housing was a force analysis using simulation tools in SolidWorks called Simulation Xpress. The main limitation of using this program was that the specific materials used for the housing were not available. Therefore, the properties of medium-high impact Acrylic, a predefined SolidWorks material, were used for the rigid Accura25 parts and the properties of Rubber, another predefined SolidWorks material, were used for the TangoPlus FullCure930 pieces. The following force distribution images were obtained from the simulation. The fixed face and the force-applied face were chosen conservatively, such that the worse-case scenario was analyzed. The force used (F=0.3924 N) was based on the product of gravitational acceleration (a=9.81 m/s^2) and the mass of the total housing (m=40 g) using the kinematic equation shown in Eq. 33.

$$F = ma \tag{33}$$

The calculated force was a conservative estimate for the actual force that the prototype may experience. In the series of images presented in Figure 36 through Figure 40, the results of the finite element analysis are depicted. The blue areas are those exhibiting the lowest stresses and have the least danger of failure while the red areas are those experiencing the great stresses and are of concern.

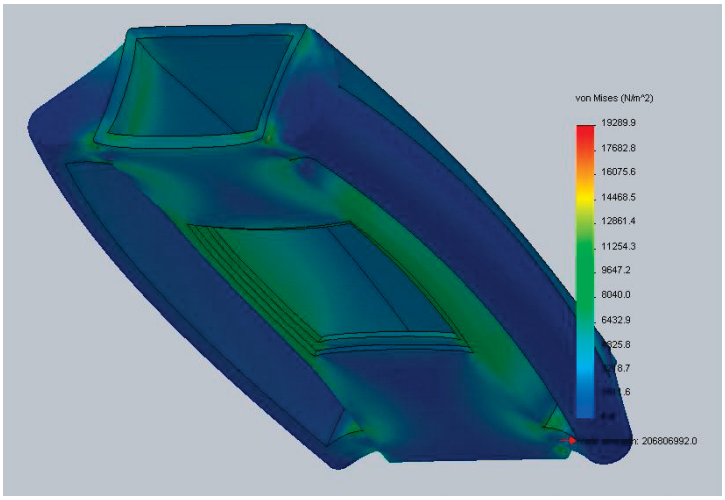

Figure 36: SolidWorks FEA analysis performed on main housing unit

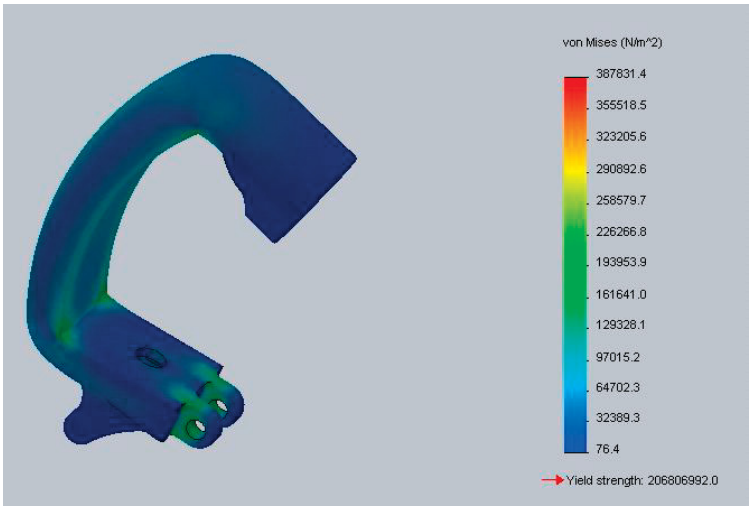

Figure 37: SolidWorks FEA analysis performed on LED arm of sensor housing

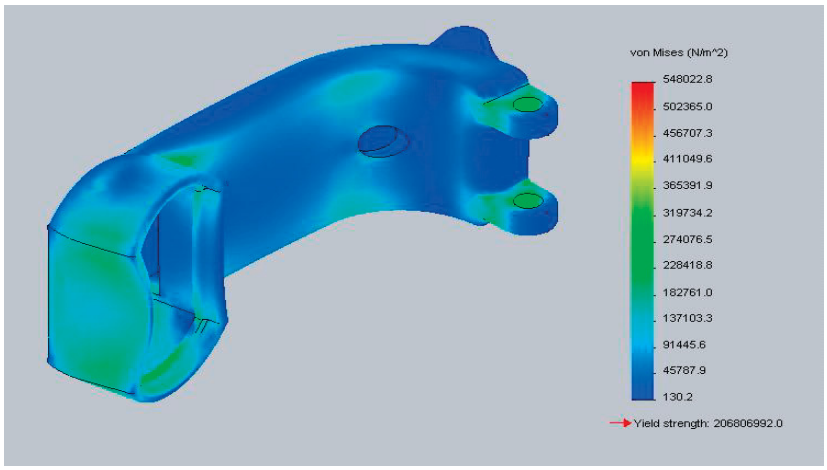

Figure 38: SolidWorks FEA analysis performed on photodiode arm of sensor housing

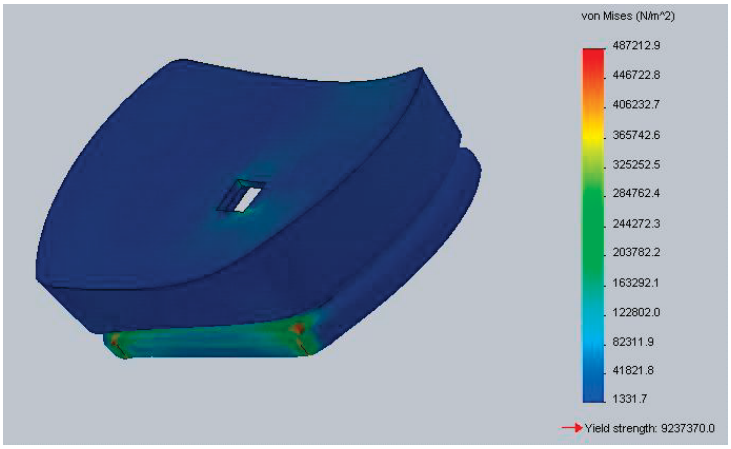

Figure 39: SolidWorks FEA analysis performed on photodiode cover

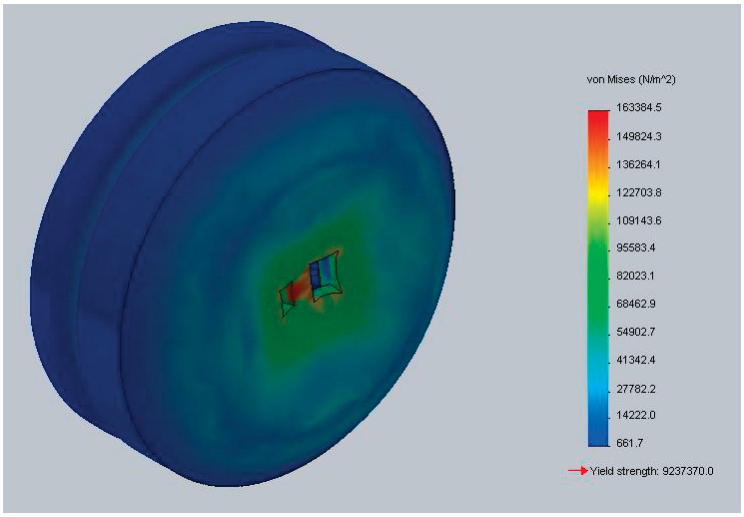

Figure 40: SolidWorks FEA analysis performed on cover for LEDs

Since the housing, in total, was incredibly light and was constructed out a very strong material in regards to the application, housing breakage was not of much concern as long as it stayed within a reasonable temperature range (temperatures usually experienced by the human body – 0 to 120°F). Please refer to the data sheets in Appendix D: Housing Material Properties for more information on the housing materials.

There was no reasonable way to test the water resistance of the housing as there was only time to develop one prototype before the completion of the project. If the time and budget was available to create multiple prototypes, then a submersion test could have been carried out to test the water resistance of the oximeter. In order not to damage the one prototype available to us, this functional requirement was not tested.

7.2 LED Driver Testing

The required functions of the LED driver were: to have a variable output current through the LEDs (ranging from 0-100mA), to have a stable output current independent of temperature, and to switch between a red and an infrared LED.

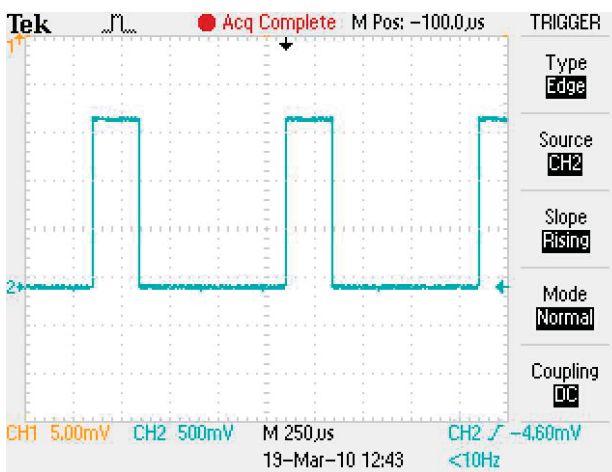

Figure 41: Voltage across the LED driver drain resistor - used for current sensing

Figure 41 illustrates the LED driver operating at 100mA. The LED driver is stable at both current levels. The LED driver was tested through the entire range of current values from 0mA to 100mA. Up to approximately 85mA, the input voltage from the microcontroller versus the LED current (V_{in}/I_{LED}) was linear. Between 85mA to 100mA, V_{in}/I_{LED} began to slowly decrease. This decrease was not significant enough to have a major effect on the linearity of V_{in}/I_{LED} and the overall functionality of the LED driver.

The transconductance of the LED driver was experimentally determined as 0.05A/V. This value illustrates the relationship between the change in output current for a given change in the input voltage. Or put simply, a 20mV change of input voltage corresponded to a 1mA change in the output current.

We have operated the LED driver continuously for extended periods of time and have observed no significant deviations in the output current. The OPA333 was chosen for the LED driver as it is a zero-drift operational amplifier whose performance has been verified by Texas Instruments. Our results were consistent with the performance claimed by TI.

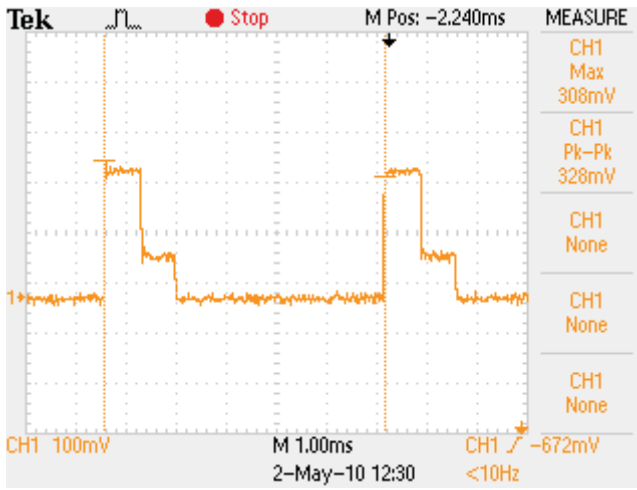

Figure 42: Red and infrared LEDs switching capability

We have tested and verified the switching capability of the LED driver between an IR and a red LED, as shown in Figure 42. The switching speed was tested up to 1kHz to ensure that its operational characteristics would be sufficient at 100Hz. The output at 1kHz, switching between the LEDs, was almost a perfect square wave, as the rise time was approximately 9ns. Thusly, the rise and fall times were negligible with regard to the signal waveform. It was possible to have small rise and fall times due to the final design including a Texas Instruments TS3A44159RSVR switch.

7.3 Transimpedance Amplifier Testing

The required functions of the transimpedance amplifier were: to precisely amplify the photodiode current to a usable voltage for the ADC (with low noise), to have a variable DC offset, and to have adjustable gain.

During breadboard testing, very high levels of noise were observed. A Yokogawa GS610 high precision current source was used to simulate the current from a photodiode. However, the current source had

an offset of 1.53µA, which was on the order of the expected signal. As such, the accuracy of the test was suspect. Significant noise injection from this current source and noise from the high capacitance breadboard contributed approximately 200mV$_{pp}$ of noise. These noise levels necessitated testing on a PCB with an actual photodiode. During testing with the final PCB and photodiode, the design and simulation in TINA-SPICE was verified by the extremely low noise levels on the output voltage signal. The detected noise was on the level of the noise floor for the oscilloscope (TDS2002B): approximately 20mV$_{pp}$. The output voltage range was 100mV to 3.3V. Below approximately 100mV, the OPA376 and OPA333 are not guaranteed to function properly. Thusly, the smallest possible output was 100mV. In Figure 43, the pulses come in pairs. For a given pair, the first pulse was due to the red LED and the second pulse was due to the IR LED. As can be seen, they were in the range of 0.8-1.22 V.

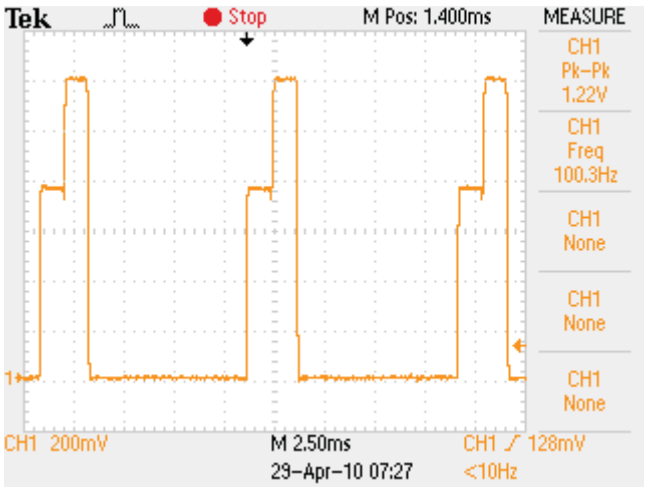

Figure 43: Voltage output from transimpedance amplifier

The variable DC offset is controlled by a microcontroller DAC. Different DC levels were applied by the DAC and the DC offset on the output was observed to change by the same level, thus confirming the correct functionality of the variable DC offset.

To test the two gain loops (gains of 2 and 10), the output voltage was observed with the stage of gain 2 enabled, followed by observation of the stage of gain 10. No input was applied; thus, the output was equal to the product of the 100mV offset on the OPA376 and the gain. Voltages of approximately 200mV and 1V were measured on the output of the transimpedance amplifier with gains 2 and 10 respectively.

It is important to note that the AC signal, representing the pulse rate of the oximeter user, is on the order of 1% of the detected DC signal [10]. Thusly, the AC signal was expected to be on the order of 1-10mV, which was below the noise floor. As can be seen in Figure 44, the AC ripple was found to be approximately 20mV. Measuring the period between peaks, the heart rate of Scott Little was calculated to be 1.398Hz or 83.84 beats/min. To verify his heart rate, Scott counted his heart beats over 15 seconds. His manually measured heart rate was 84 beats/min.

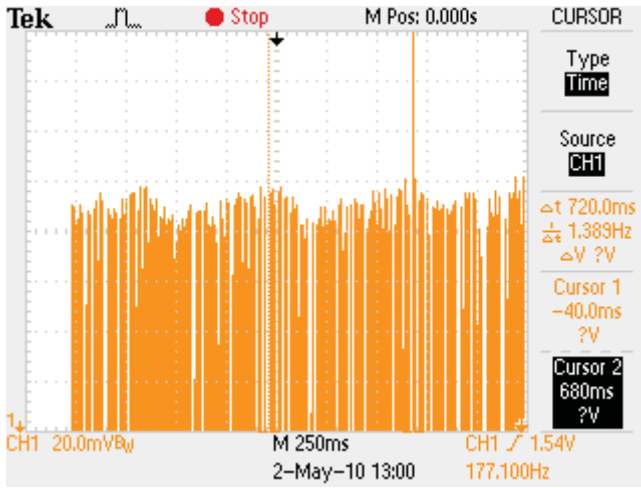

Figure 44: AC ripple representing pulse rate

7.4 Microcontroller Testing

The required functions of the microcontroller were: control the LED driver, acquire data from the transimpedance amplifier, and send data to the user interface.

The microcontroller controlled a DAC that is a voltage input to the LED driver, which controlled the output current (therefore the intensity) of the LEDs. This was verified by measuring the output voltages for the DAC and also from the LED driver testing. In addition, the microcontroller controlled the switching of the LEDs. This was verified by measuring the voltage applied on the switch using an oscilloscope (TDS2002B).

The transimpedance amplifier outputted a voltage to the ADC, which was read by the microcontroller. The microcontroller also sent a control signal to the gain stage to adjust the gain and ensure the signal fell within the desired range. In addition, the microcontroller applied a DC offset to the signal. Both the gain control and DC offset control were verified in the testing of the transimpedance amplifier.

The data was sent to the user interface from the microcontroller. To ensure proper functionality of the data transmission, the TDS2002B oscilloscope was used to analyze the logic signals being sent from the microcontroller. Upon verification of the logic signals, a known set of data was sent from the pulse oximeter microcontroller to the USB receiver connected to a personal computer. The received data was viewed in HyperTerminal to verify that the data was correctly received. Data transmission to the iPhone was verified during user interface testing.

7.5 User Interface Testing

The required functions of the user interface were: to display the SpO_2 and heart rate, to sound an alert for low SpO_2 levels, and to perform data logging.

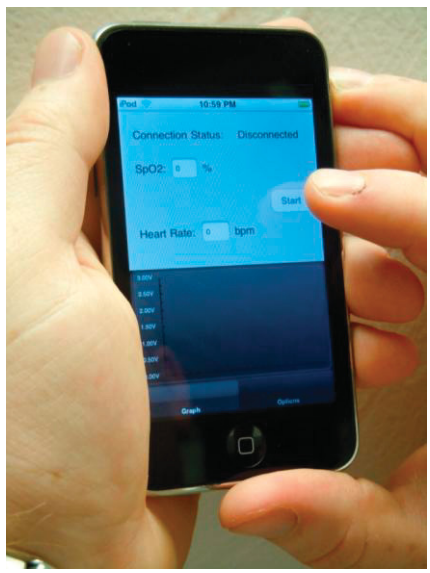

Figure 45: Final iPhone interface

To verify that the SpO_2 display functioned properly, SpO_2 data was sent to the iPhone and the reading on the display was observed to change accordingly. Figure 45 shows the final interface design being utilized by a user.

To test the alert signal, data corresponding to a low SpO_2 was sent to the iPhone. Following SpO_2 calculations, the alert signal was triggered as expected.

To verify the data logging functionality, data was sent to the iPhone from the USB wireless receiver and saved to a temporary file. The file was then uploaded to an FTP server which was read by a personal laptop.

8 Conclusions & Recommendations

The remote pulse oximeter project has resulted in a functional design that fulfilled all of the major functional requirements, as well as Texas Instruments' request for a reference design for future customers in the medical device field. The unit is powered from a readily available 2032 battery, which is already widely implemented in several other medical devices. The form factor of the housing is such that it mitigates ambient light noise, protects the vital circuitry from damage in day-to-day use, and the novel ear-clip design is compatible with a wide range of potential users. In terms of functionality, the oximeter was able to output the user's $Sp0_2$ level, with an accuracy comparable with commercial-grade sensors, in addition to dynamically calculating and displaying the user's heart rate. The oximeter hardware was able to transmit data wirelessly, and can do so through any existing WiFi network. Lastly, the novel iPhone OS-based user interface proved to be a simple means of acquiring and displaying data, and due to the growing popularity of Apple's iPhone and iPod touch, is currently available to over 70 million consumers.

Despite the success of this first-generation project, there is room for improvement in a number of areas of this project. The use of smaller electronics packages could result in a smaller PCB, and hence, a smaller overall housing. With enough design iterations, all of the electrical components could potentially be integrated into the ear-clip portion of the housing, significantly reducing the overall form factor of the device. The use of a higher supply voltage, thus necessitating a larger battery or voltage regulator, would improve the quality of the output signal by making the AC signal easier to measure. Modifying the analog circuitry to perform sample and hold functions would allow the separation of the vital signals into separate channels; AC and DC could be separated, as well as the red and IR signals. The use of multiple channels could result in higher resolution of the individual signals, ultimately increasing the overall accuracy of the device.

Even without the aforementioned improvements, this pulse oximeter design has demonstrated that not only is it fully functional as a stand-alone device, but also that it could potentially be commercialized by Texas Instruments. The most expensive portions of this prototype, being the rapid-prototyped housing and PCB fabrication and population, would be significantly reduced if ordered in large numbers. Further, nearly all of the analog components are produced by Texas Instruments, further reducing cost. Expanding the user interface to include both PCs, Macs, as well as other smart-phone operating systems, such as Google Android, Palm WebOS, and Blackberry devices would account for a much larger

percentage of the target consumer audience, reducing design costs associated with creating a proprietary user interface system.

9 Acknowledgements

Project Sponsor:

Texas Instruments

Matthew Hann	*HPA Linear Applications Engineer*

ENGR498 Mentor:

Fred Highton

Departmental Advisors:

Michael Descour	*College of Optical Sciences*
Charles Higgins	*Neuroscience*
Ali Akoglu	*Electrical/Computer Engineering*
Jeong –Yeol Yoon	*Agriculture/Biosystems Engineering*

Companies Providing Components/Services:

Texas Instruments	*Develops analog, digital signal processing, RF, and DLP*
Kingbright	*LED manufacturer*
Advanced Photonix	*Opto-Electronics manufacturer*
Fairchild	*Semiconductor manufacturer*
Sierra Proto Express	*Printed circuit board manufacturer*
360 Prototyping	*Supplier of rapid- prototyped components*

10 References

1. Billauer, Eli. "Peakdet: Peak Detection Using MATLAB." *Eli Billauer's Home Page*. Web. <http://www.billauer.co.il/peakdet.html>.

2. "Core-Plot." *Google Code*. Web. <http://code.google.com/p/core-plot/>.

3. Kyriacou, P. A. "Pulse Oximetry in the Oesophagus." *Physiological Measurement* 27.1 (2006). Web.

4. Li, Yun-Thai. "Pulse Oximetry." Web. <http://personal.ph.surrey.ac.uk/~phs3ps/surj/v2/li.pdf>.

5. Prahl, Scott. "Optical Absorption of Hemoglobin." *Laser Photomedicine and Biomedical Optics at the Oregon Medical Laser Center*. Web. <http://omlc.ogi.edu/spectra/hemoglobin/index.html>.

6. "SimpleFTPSample." *Apple Developer*. Web. <http://developer.apple.com/iphone/library/samplecode/SimpleFTPSample/Introduction/Intro.html>.

7. "SimpleNetworkStreams." *Apple Developer*. Web. <http://developer.apple.com/iphone/library/samplecode/SimpleNetworkStreams/>.

8. "Understanding Pulse Oximetry SpO2 Concepts." *Philips Medical Systems*. Web. <http://incenter.medical.philips.com/doclib/enc/fetch/586262/586457/Understanding_Pulse_Oximetry.pdf%3Fnodeid=586458&vernum=2>.

9. "U.S. Home Size — Infoplease.com." *Infoplease: Encyclopedia, Almanac, Atlas, Biographies, Dictionary, Thesaurus. Free Online Reference, Research & Homework Help. — Infoplease.com*. Web. <http://www.infoplease.com/askeds/us-home-size.html>.

10. Webster, John G. *Design of Pulse Oximeters*. Bristol: Institute of Physics Pub., 1997. Print.

11 Appendix A: Main Component List

	Name/Description	Manufacturer	Part #
Housing	Black ABS/Black Rubber	360 Prototyping	N/A
Source/Detector	Surface Mount PIN Photodiode	Advanced Photonix	PDB-C154SM
	Red Surface Mount LED	Kingbright	APG1608SURKC/T
	IR Surface Mount LED	Kingbright	APT1608F3C
LED Driver/ Temp Sensor	Remote Temperature Sensor	Texas Instruments	TMP411
	CMOS Low Voltage Op Amp	Texas Instruments	OPA333
	Quad SPDT Analog Switch	Texas Instruments	TS3A44159
	PNP Transistor	Fairchild	PN2907
Transimpedance Amplifier	Low Noise Op Amp	Texas Instruments	OPA376
	CMOS Low Voltage Op Amp	Texas Instruments	OPA333
Microcontroller	Surface Mount MCU	Texas Instruments	MSP430FG477
	RF Transceiver	Texas Instruments	CC2500
	Analog to Digital Converter	Texas Instruments	ADS1015
User Interface	iPod Touch	Apple	N/A

12 Appendix B: Bill of Materials

Subassembly	Part No.	Description	Manufacturer	Qty	Price Each	Subtotal
Housing	PROTO	Ear Back Housing	360 Prototyping	1	$25.00	$25.00
	PDB-C154SM	Ear Front Housing	360 Prototyping	1	$26.00	$26.00
	N/A	Main Battery Cover	360 Prototyping	1	$23.00	$23.00
	N/A	Main Cap	360 Prototyping	1	$12.00	$12.00
	N/A	Main House	360 Prototyping	1	$185.00	$185.00
	N/A	Silicone Insert Convex Detect	360 Prototyping	1	$132.00	$132.00
	N/A	Silicone Insert Convex LED's	360 Prototyping	1	$75.00	$75.00
Source/ Detector	APG1608SURKC/T	Red Surface Mount LED	Kingbright	1	$0.30	$0.30
	APT1608F3C	IR Surface Mount LED	Kingbright	1	$0.26	$0.26
	PDB-C154SM	Photodiode	Advanced Photonix Inc	1	$2.34	$2.34
LED Driver	OPA2333AIDRBT	CMOS Low Voltage Op Amp	Texas Instruments	1	$2.00	$2.00
	TS3A44159RSVR	Switch	Texas Instruments	1	$0.52	$0.52
	TMP411ADGKR	Temperature Sensor	Texas Instruments	1	$1.40	$1.40
	MMBT2907A-TP	PNP Transistor	Micro Commercial Co	1	$0.32	$0.32
	RP1005S-100-F	Resistor 10Ω	Susumu	10	$0.50	$5.00
	ERJ-2RKF1000X	Resistor 100Ω	Panasonic - ECG	10	$0.10	$1.00
	ERJ-2RKF1001X	Resistor 1kΩ	Panasonic - ECG	10	$0.10	$0.98
	ERJ-2RKF1002X	Resistor 10kΩ	Panasonic - ECG	10	$0.10	$1.00
	ERJ-2RKF1003X	Resistor 100kΩ	Panasonic - ECG	10	$0.10	$1.00
	ERJ-2RKF1243X	Resistor 125kΩ	Panasonic - ECG	10	$0.10	$1.00
	GRM1885C1H202JA01D	Capacitor 2nF	Murata Electronics	1	$0.08	$0.08
	C0402C104K8PACTU	Capacitor 100nF	C0402C104K8PACTU	7	$0.02	$0.14
Interface	MB528LL/A	iPod Touch (8GB)	Apple	1	$189.00	$189.00
	APPDEVSDK	iPhone Software Developer Kit	Apple	1	$99.00	$99.00
	MSP430FG477	MSP430 Microcontroller	Texas Instruments	1	$5.55	$5.55
	ADC1015	A2D Converter	Texas Instruments	1	$5.54	$5.54
	CC2500	RF Sensor	Texas Instruments	1	$3.83	$3.83
	PGA204	Programmable Gain Amp	Texas Instruments	1	$16.58	$16.58
	TPS60120	Power Mgmt IC	Texas Instruments	1	$3.60	$3.60
	PCBEXPRESSQ4	Printed Circuit Board	Sierra Circuits	1	$107.00	$107.00
	PCBPOP	PCB Population	Sierra Circuits	1	$50.00	$50.00

Subassembly	Part No.	Description	Manufacturer	Qty	Price Each	Subtotal
Amplifier	OPA376AIDBVT	OP Amp /OPA376	Texas Instruments	1	$1.50	$1.50
	OPA333AIDCKT	OP Amp /OPA333	Texas Instruments	1	$1.94	$1.94
	OPA344	Capacitor Bootstrapping	Texas Instruments	1	$1.55	$1.55
	NSWC	Low ESR capacitor	NIC Components	10	$1.25	$12.50
	PTF56	Metal Film Resistor	Vishay	50	$0.40	$20.00
	TS5A4624DCKR	Switch	Texas Instruments	1	$0.20	$0.20
	ERA-3AEB102V	Resistor 1kΩ	Panasonic - ECG	1	$0.20	$0.20
	ERA-3AEB472V	Resistor 4.7kΩ	Panasonic - ECG	1	$0.20	$0.20
	ERA-3AEB512V	Resistor 5.1kΩ	Panasonic - ECG	2	$0.20	$0.40
	ERA-3AEB103V	Resistor 10kΩ	Panasonic - ECG	1	$0.20	$0.20
	ERA-3AEB393V	Resistor 39kΩ	Panasonic - ECG	1	$0.20	$0.20
	ERA-3AEB513V	Resistor 51kΩ	Panasonic - ECG	1	$0.20	$0.20
	ERA-6AEB105V	Resistor 1MΩ	Panasonic - ECG	1	$0.20	$0.20
	C1005C0G1H160J	Capacitor 15pF	TDK Corporation	1	$0.02	$0.02
	04025C391JAT2A	Capacitor 390pF	AVX Corporation	1	$0.42	$0.42
	GRM1885C1H162JA01D	Capacitor 1.6nF	Murata Electronics	1	$0.08	$0.08
	LMK105SD332JV-F	Capacitor 3.3nF	Taiyo Yuden	1	$0.43	$0.43
	0402YC153KAT2A	Capacitor 15nF	ManufacturerAVX	1	$0.11	$0.11
	C0402C104K8PACTU	Capacitor 100nF	Kemet	3	$0.02	$0.07
Microcontroller	ADS1015IRUGT	ADC	Texas Instruments	1	$2.68	$2.68
	CC2500RTKR	RF Tranceiver	Texas Instruments	1	$2.26	$2.26
	MSP430F1612IRTDT	MSP430	Texas Instruments	1	$13.33	$13.33
	TPS63001	Regulator	Texas Instruments	1	$2.00	$2.00
	7488910245	Antenna	Wurth Electronics Inc	1	$4.80	$4.80
	ABM3B-26.000MHZ-10-1-U-T	Crystal	Abracon Corporation	1	$2.63	$2.63
	ERJ-2RKF5602X	Resistor 56kΩ	Panasonic - ECG	1	$0.10	$0.10
	ERJ-2RKF1002X	Resistor 10kΩ	Panasonic - ECG	3	$0.10	$0.29
	ERJ-2RKF4702X	Resistor 47kΩ	Panasonic - ECG	1	$0.10	$0.10
	ERJ-2GEJ114X	Resistor 110kΩ	Panasonic - ECG	1	$0.08	$0.08
	C0402C104K8PACTU	Capacitor 100nF	Kemet	12	$0.02	$0.29
	GRM1555C1H270JZ01D	Capacitor 27pF	Murata Electronics	2	$0.02	$0.04
	GRM1555C1H101JZ01D	Capacitor 100pF	Murata Electronics	5	$0.02	$0.08
	ECJ-0EC1H010C	Capacitor 1pF	Panasonic - ECG	2	$0.08	$0.16
	ECD-G0ER508	Capacitor .47pF	Panasonic - ECG	2	$0.42	$0.84
	ECJ-1VB0J106M	Capacitor 10µF	Panasonic - ECG	2	$0.45	$0.90
	ELJ-RF4N7DFB	Inductor 4.7nH	Panasonic - ECG	3	$0.08	$0.24
	MLF1005A1R0KT	Inductor 1µH	TDK Corporation	1	$0.60	$0.60
	MLF1005A2R2KT	Inductor 2.2µH	TDK Corporation	1	$0.60	$0.60
					Total	**$1,047.88**

13 Appendix C: Project Budget/Expenses

Category	Description	Funding Source	Amount Budgeted	Amount Spent	Remainder
Components	LED Driver	ENGR 498A	$ 25.00	$ 17.34	$ 7.66
	Transimpedance Amplifier		$ 50.00	$ 40.42	$ 9.58
	Wireless Transmission		$ 100.00	$ 67.12	$ 32.88
	User Interface		$ 220.00	$ 199.00	$ 21.00
	Housing		$ 800.00	$ 478.00	$ 322.00
	PCB Fabrication		$ 600.00	$ 725.00	$ (125.00)
Equipment	Precision Voltage Source	Sponsor	$ -	$ -	$ -
	Precision DMM				
	Oscilloscope				
	Function Generator				
	Logic Analyzer				
	USB Microcontroller				
	A/D Converter Evaluation Module				
Software	iPhone Application Development Software	ENGR 498A	$ 110.00	$ 106.52	$ 3.48
Shipping	Shipping Expenses	ENGR 498A	$ 200.00	$ 212.60	$ (12.60)
Presentation	Design Day Poster	ENGR 498A	$ 150.00	$ 128.52	$ 21.48
Miscellaneous	Contingency Funds	ENGR 498A	$ 745.00	$ -	$ 745.00

Total Budgeted **$ 3,000.00**

Total Spent **$ 1,974.52**

Total Remaining **$ 1,025.48**

14 Appendix D: Housing Material Properties

3D SYSTEMS

Accura® 25 plastic

for use with solid-state stereolithography (SLA®) systems

Simulate the properties and aesthetics of polypropylene with this accurate and flexible material.

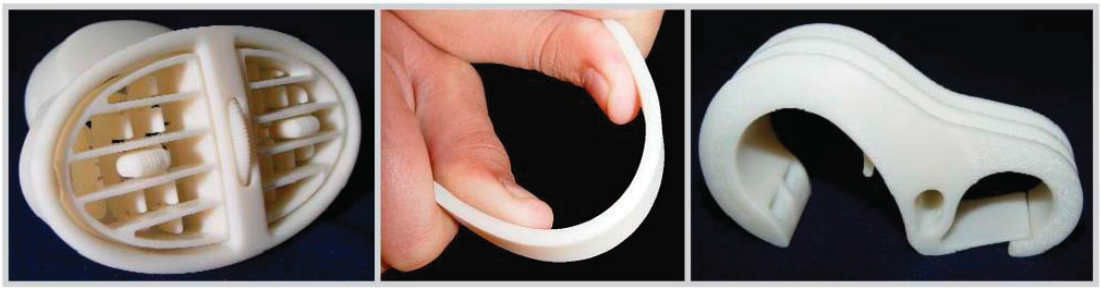

APPLICATIONS

- Functional components for assemblies and mock-ups for:
  - Automotive styling parts — trim, fascia, and other components
  - Consumer electronic components
  - Toys
  - Snap fit assemblies
- Master patterns for RTV/silicone molding
- Replace CNC machining of polypropylene to produce short-run plastic parts
- Simulate injection molded parts
- Concept and marketing models

FEATURES

- Look and feel of molded polypropylene
- High flexibility with excellent shape retention
- Outstanding feature resolution and accuracy
- High production speed
- Fully developed and tested build styles

BENEFITS

- Increased market opportunities for models
- Reliable and robust functional prototypes
- Suitable for master patterns
- More parts and better system utilization
- Maximize reliability with no user R&D

3D SYSTEMS CORPORATION

TRANSFORM YOUR PRODUCTS

Accura® 25 plastic

For use with all solid-state stereolithography (SLA®) systems

"After providing some models in Accura 25 to a couple of our regular customers, they have decided to make it their default SL material for all future orders. To date they have already ordered hundreds of parts. They get a material that looks like a final article molded part having a great balance of durability and flexibility. I get a material that is very easy to clean and finish, but most importantly is extremely reliable in the machine. This has been a real win-win for us.."

— Steve Grundahl — Owner, Midwest Prototyping LLC

TECHNICAL DATA

Liquid Material

MEASUREMENT	METHOD/CONDITION	VALUE
Appearance		White
Liquid Density	@ 25 °C (77 °F)	1.13 g/cm³
Solid Density	@ 25 °C (77 °F)	1.19 g/cm³
Viscosity	@ 30 °C (86 °F)	250 cps
Penetration Depth (Dp) *		4.2 mils
Critical Exposure (Ec) *		10.5 mJ/cm²
Tested Build Styles		FAST™, EXACT™, Exact HR

Post-Cured Material

MEASUREMENT	METHOD/CONDITION	METRIC	U.S.
Tensile Strength	ASTM D 638	38 MPa	5,450 - 5,570 PSI
Tensile Modulus	ASTM D 638	1,590 - 1,660 MPa	230 - 240 KSI
Elongation at Break (%)	ASTM D 638	13 - 20 %	
Flexural Strength	ASTM D 790	55 - 58 MPa	7,960 - 8,410 PSI
Flexural Modulus	ASTM D 790	1,380 - 1,660 MPa	200 - 240 KSI
Impact Strength (Notched Izod)	ASTM D 256	19-24 J/m	0.4 ft- lb/in
Heat Deflection Temperature	ASTM D 648 @ 66 PSI @ 264 PSI	 58 - 63 °C 51 - 55 °C	 136 - 145 °F 124 - 131 °F
Hardness, Shore D		80	
Co-efficient of Thermal Expansion	ASTM E 831-93 TMA (T<Tg, 0 - 20 °C) TMA (T>Tg, 90 - 150 °C)	 107×10^{-6} m/m °C 151×10^{-6} m/m °C	
Glass Transition (Tg)	DMA, E″	60 °C	140 °F

* Dp/Ec values are the same on all systems.

SYSTEMS

TRANSFORM YOUR PRODUCTS

3D Systems Corporation
333 Three D Systems Circle
Rock Hill, SC 29730 U.S.A.

Tel: 803.326.4080
Toll-free: 800.889.2964
Fax: 803.324.8810

moreinfo@3dsystems.com
www.3dsystems.com
NASDAQ: TDSC

Warranty/Disclaimer: The performance characteristics of these products may vary according to product application, operating conditions, material combined with, or with end use. 3D Systems makes no warranties of any type, express or implied, including, but not limited to, the warranties of merchantability or fitness for a particular use.

© 2007 by 3D Systems, Inc. All rights reserved. Specifications subject to change without notice. The 3D logo, Accura and SLA are registered trademarks of 3D Systems, Inc.

PN 70668 Issue Date • 06 Sep 07

FullCure Materials

Support Your Application

- Elongation at break of 20% and 44% for rigid models enables fit and function
- Elongation at break of 47% and 218% for rubber-like materials
- Models ready to use, no extra finishing required
- Models can be handled right off the tray
- Paint readily adheres to model surfaces
- Easy to remove gel-like support material ensures no hard grid edges
- Single support material for all materials
- High accuracy models

OBJET

Support your Applications

The FullCure® line of photopolymer resins open up a whole world of possibilities for users of 3-dimensional printings.

Based on Objet's unique ultra-thin-layer Polyjet™ technology, FullCure® resins are used to create accurate, highly detailed three-dimensional models for a wide range of applications. Unlike models created by other technologies, Objet-made parts are fully cured during the build process and can be handled immediately after build.

The FullCure® line includes several types of flexible and rigid model materials. The FullCure® support material enables users to produce any geometry, including overhangs and undercuts.

The FullCure® line currently includes the following materials, with more to come in the near future:

FullCure®720 -General-purpose resin, offers excellent technical properties in a transparent color.

Vero materials - Feature opaque colors and improved mechanical properties, offering users excellent detail visualization and even wider range of applications.

Tango materials - offer users highly flexible materials with different levels of elasticity, enabling a close "touch and feel" match for any design.

Key Advantages

- Elongation at break of 20% for rigid models enables fit and function.
- Elongation at break of 47% and 218% for rubber-like materials.
- Models ready to use, no extra finishing required.
- Models can be handled right off the tray.
- Paint readily adheres to model surfaces.
- Easy to remove gel-like support materials ensures no hard grid edges.
- Single support material for all materials.
- High accuracy models.

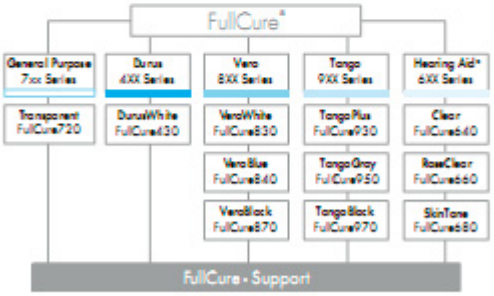

*See Objet Hearing Aid brochure

Tango

TangoPlus - FullCure930

Property	ASTM	Metric		Imperial	
Tensile Strength at Break	D-412	MPa	1.455	psi	211
Tensile Modulus at 20% Strain	D-413	MPa	0.146	psi	21
Tensile Modulus at 30% Strain	D-414	MPa	0.185	psi	27
Tensile Modulus at 50% Strain	D-415	MPa	0.263	psi	38
Elongation at Break	D-412	%	218	%	218.0
Compressive Set, 22 Hr, 75OC	D-395	%	4.4	%	4.4
Shore A Hardness	D-2240	Scale A	27	Scale A	27
Ross Flex	D-1052		Above 150,000		Above 150,000
Tensile Tear Resistance	D-624	Kg/cm	3.47	Lb/in	20
Tg	DSC (-80°C+100°C)	C°	-9.6	F°	15

TangoGray - FullCure950

Property	ASTM	Metric		Imperial	
Tensile Strength	D-412	MPa	4.36	psi	632
Elongation at Break	D-412	%	47	%	47.0
Compressive Set	D-395	%	1	%	1
Shore A Hardness	D-2240	Scale A	75	Scale A	75
Tensile Tear Resistance	D-624	Kg/cm	9.5	Lb/in	54
Tg	DSC (-80°C+100°C)	C°	2.6	F°	37

TangoBlack - FullCure970

Property	ASTM	Metric		Imperial	
Tensile Strength	D-412	MPa	2	psi	290
Elongation at Break	D-412	%	47.7	%	47.7
Compressive Set	D-395	%	0.8	%	1
Shore A Hardness	D-2240	Scale A	61	Scale A	61
Tensile Tear Resistance	D-624	Kg/cm	3.8	Lb/in	21
Tg	DSC (-80°C+100°C)	C°	10.7	F°	13

FullCure Materials

Vero

VeroWhite - FullCure830

Property	ASTM	Metric		Imperial	
Tensile Strength	D-638-03	MPa	49.8	psi	7221
Modulus of Elasticity	D-638-04	MPa	2495	psi	361775
Elongation at Break	D-638-05	%	20	%	20
Flexural Strength	D-790-03	MPa	74.6	psi	10817
Flexural Modulus	D-790-04	MPa	2137	psi	309865
Izod Notched Impact	D-256-06	J/m	24.1	ft lb/in	0.45
Shore Hardness	Scale D	Scale D	83	Scale D	83
Rockwell Hardness	Scale M	Scale M	81	Scale M	81
HDT at 0.45 MPa	D-648-06	C°	43	F°	109
HDT at 1.82 MPa	D-648-07	C°	40	F°	104
Tg	DMA, E"	C°	58	F°	136
Ash Content	NA	%	<0.4	%	<0.4
Water Absorption	D570-98 24 Hr	%	1.15	%	1.15

VeroBlue - FullCure840

Property	ASTM	Metric		Imperial	
Tensile Strength	D-638-03	MPa	55.1	psi	7990
Modulus of Elasticity	D-638-04	MPa	2740	psi	397300
Elongation at Break	D-638-05	%	20	%	20
Flexural Strength	D-790-03	MPa	83.6	psi	12122
Flexural Modulus	D-790-04	MPa	1983	psi	287535
Compressive Strength	D-695-02	MPa	79.3	psi	11499
Izod Notched Impact	D-256-06	J/m	23.6	ft lb/in	0.44
Shore Hardness	Scale D	Scale D	83	Scale D	83
Rockwell Hardness	Scale M	Scale M	81	Scale M	81
HDT at 0.45 MPa	D-648-06	C°	48.8	F°	120
HDT at 1.82 MPa	D-648-07	C°	44.8	F°	113
Tg	DMA, E"	C°	48.7	F°	120
Ash Content	NA	%	<0.3	%	<0.3
Water Absorption	D570-98 24 Hr	%	1.54	%	1.54

VeroBlack - FullCure870

Property	ASTM	Metric		Imperial	
Tensile Strength	D-638-03	MPa	50.7	psi	7352
Modulus of Elasticity	D-638-04	MPa	2192	psi	317840
Elongation at Break	D-638-05	%	17.7	%	18
Flexural Strength	D-790-03	MPa	79.6	psi	11542
Flexural Modulus	D-790-04	MPa	2276	psi	330020
Izod Notched Impact	D-256-06	J/m	23.9	ft lb/in	0.45
Shore Hardness	Scale D	Scale D	83	Scale D	83
Rockwell Hardness	Scale M	Scale M	81	Scale M	81
HDT at 0.45 MPa	D-648-06	C°	47	F°	117
HDT at 1.82 MPa	D-648-07	C°	42.9	F°	109
Tg	DMA, E"	C°	62.7	F°	145
Water Absorption	D570-98 24 Hr	%	1.01	%	1.01

General Purpose

FullCure720

Property	ASTM	Metric		Imperial	
Tensile Strength	D638-03	MPa	60.3	psi	8744
Modulus of Elasticity	D638-04	MPa	2870	psi	416150
Elongation at Break	D638-05	%	20	%	20
Flexural Strength	D790-03	MPa	75.8	psi	10991
Flexural Modulus	D790-04	MPa	1718	psi	249110
Compressive Strength	D695-02	MPa	84.3	psi	12224
Izod Notched Impact	D256-06	J/m	23.6	ft lb/in	0.44
Shore Hardness	Scale D	Scale D	83	Scale D	83
Rockwell Hardness	Scale M	Scale M	81	Scale M	81
HDT at 0.45 MPa	D648-06	C°	48.4	F°	119
HDT at 1.82 MPa	D648-07	C°	44.4	F°	112
Tg	DMA, E"	C°	48.7	F°	120
Ash Content	NA	%	<0.01	%	<0.01
Water Absorption	D57098 24 Hr	%	1.53	%	1.53

Durus

DurusWhite - FullCure430

Property	ASTM	Metric		Imperial	
Tensile Strength	D-638-03	MPa	21.3	psi	3089
Modulus of Elasticity	D-638-04	MPa	1135.8	psi	164691
Elongation at Break	D-638-05	%	44.2	%	44
Flexural Strength	D-790-03	MPa	33.2	psi	4814
Flexural Modulus	D-790-04	MPa	1026.1	psi	148785
Compressive Strength	D-695-02	MPa	30.7	psi	4452
Izod Notched Impact	D-25606	J/m	44.22	ft lb/in	0.83
Shore Hardness	D-2240-03	Scale D	76	Scale D	76
Rockwell Hardness	D-785-03	Scale M	97	Scale M	97
HDT at 0.45 MPa	D-648-06	C°	36.3	F°	98
HDT at 1.82 MPa	D-648-07	C°	32.6	F°	91
Tg	DMA, E"	C°	35.9	F°	97
Water Absorption	D57098 24 Hr	%	1.69	%	1.69

Objet Geometries Ltd.
Headquarters
2 Holzman st.,
Science Park,
P.O Box 2496,
Rehovot76124, Israel
T: +972-8-931-4314
F: +972-8-931-4315

Objet Geometries Inc.
North America
5 Fortune Drive
Billerica,
MA 01821
USA
T: +1-877-489-9449
F: +1-866-676-1533

Objet Geometries
GMBH
Im Leuschnerpark 4,
64347 Griesheim
Germany
T: +49-6155-605-346
F: +49-6155-605-344

Objet Geometries AP
Asia Pacific
13th floor, Unit52A,
HITEC
1 Trademart Drive
Kowloon Bay, Hong Kong
T: +852-217-40111
F: +852-217-40555

Objet Geometries AP
Limited China Rep Office
Rm1220, CIMIC Tower,
1090 Century Blvd,
Pudong Shanghai
2000120 P. R. China
T: +86-21-5836-2468
F: +86-21-5836-2469

info@objet.com www.objet.com

©2008 Objet, Quadra, QuadraTempo, PolyJet, FullCure, SHR, Eden, Eden250, Eden260, Eden330, Eden350, Eden350V, Eden500V, job Manager, Objet Studio, Connex, Connex500, PolyJag, TangoBlack, TangoGray, TangoPlus, VeroBlue, VeroWhite, VeroBlack, DigitalMaterialsand PolyjetMatrixare trademarks of Objet Geometries Ltd. and may be registered in certain jurisdictions. All farther trademarks belong to their respective owners.

15 Appendix E: Microcontroller Source Code

```
//*****************************************************************************
// THIS PROGRAM IS PROVIDED "AS IS". TI MAKES NO WARRANTIES OR
// REPRESENTATIONS, EITHER EXPRESS, IMPLIED OR STATUTORY,
// INCLUDING ANY IMPLIED WARRANTIES OF MERCHANTABILITY, FITNESS
// FOR A PARTICULAR PURPOSE, LACK OF VIRUSES, ACCURACY OR
// COMPLETENESS OF RESPONSES, RESULTS AND LACK OF NEGLIGENCE.
// TI DISCLAIMS ANY WARRANTY OF TITLE, QUIET ENJOYMENT, QUIET
// POSSESSION, AND NON-INFRINGEMENT OF ANY THIRD PARTY
// INTELLECTUAL PROPERTY RIGHTS WITH REGARD TO THE PROGRAM OR
// YOUR USE OF THE PROGRAM.
//
// IN NO EVENT SHALL TI BE LIABLE FOR ANY SPECIAL, INCIDENTAL,
// CONSEQUENTIAL OR INDIRECT DAMAGES, HOWEVER CAUSED, ON ANY
// THEORY OF LIABILITY AND WHETHER OR NOT TI HAS BEEN ADVISED
// OF THE POSSIBILITY OF SUCH DAMAGES, ARISING IN ANY WAY OUT
// OF THIS AGREEMENT, THE PROGRAM, OR YOUR USE OF THE PROGRAM.
// EXCLUDED DAMAGES INCLUDE, BUT ARE NOT LIMITED TO, COST OF
// REMOVAL OR REINSTALLATION, COMPUTER TIME, LABOR COSTS, LOSS
// OF GOODWILL, LOSS OF PROFITS, LOSS OF SAVINGS, OR LOSS OF
// USE OR INTERRUPTION OF BUSINESS. IN NO EVENT WILL TI'S
// AGGREGATE LIABILITY UNDER THIS AGREEMENT OR ARISING OUT OF
// YOUR USE OF THE PROGRAM EXCEED FIVE HUNDRED DOLLARS
// (U.S.$500).
//
// Unless otherwise stated, the Program written and copyrighted
// by Texas Instruments is distributed as "freeware".  You may,
// only under TI's copyright in the Program, use and modify the
// Program without any charge or restriction.  You may
// distribute to third parties, provided that you transfer a
// copy of this license to the third party and the third party
// agrees to these terms by its first use of the Program. You
// must reproduce the copyright notice and any other legend of
// ownership on each copy or partial copy, of the Program.
//
// You acknowledge and agree that the Program contains
// copyrighted material, trade secrets and other TI proprietary
// information and is protected by copyright laws,
// international copyright treaties, and trade secret laws, as
// well as other intellectual property laws.  To protect TI's
// rights in the Program, you agree not to decompile, reverse
// engineer, disassemble or otherwise translate any object code
// versions of the Program to a human-readable form.  You agree
// that in no event will you alter, remove or destroy any
// copyright notice included in the Program.  TI reserves all
// rights not specifically granted under this license. Except
```

```
// as specifically provided herein, nothing in this agreement
// shall be construed as conferring by implication, estoppel,
// or otherwise, upon you, any license or other right under any
// TI patents, copyrights or trade secrets.
//
// You may not use the Program in non-TI devices.
//
//******************************************************************************
//   eZ430-RF2500 Temperature Sensor End Device
//
//   Description: This is the End Device software for the eZ430-2500RF
//                Temperature Sensing demo
//
//
//   L. Westlund
//   Version    1.02
//   Texas Instruments, Inc
//   November 2007
//   Built with IAR Embedded Workbench Version: 4.09A
//******************************************************************************
//Change Log:
//******************************************************************************
//Version:  1.02
//Comments: Changed Port toggling to abstract method
//          Fixed comment typos
//Version:  1.01
//Comments: Added support for SimpliciTI 1.0.3
//          Added Flash storage/check of Random address
//          Moved LED toggle to HAL
//Version:  1.00
//Comments: Initial Release Version
//******************************************************************************

#include "bsp.h"
#include "mrfi.h"
#include "nwk_types.h"
#include "nwk_api.h"
#include "bsp_leds.h"
#include "bsp_buttons.h"
#include "vlo_rand.h"
#include "mrfi_board_defs.h"
#include "msp430xG47x.h"

volatile unsigned int i;
  float ADC;
int RxData;
unsigned int results;
```

```
#define NUM_BYTES_TX 1                    // How many bytes?

int RXByteCtr, RPT_Flag = 0;              // enables repeated start when 1
volatile unsigned char RxBuffer[12];        // Allocate 128 byte of RAM
unsigned char *PTxData;                   // Pointer to TX data
unsigned char TXByteCtr;
unsigned char MSData = 0x01;

void Setup_TX(void);
void Transmit(void);
void Receive(void);

void linkTo(void);
void MCU_Init(void);

__no_init volatile int tempOffset @ 0x10F4; // Temperature offset set at production
__no_init volatile char Flash_Addr[4] @ 0x10F0; // Flash address set randomly

void createRandomAddress();
void i2cconfig3();
void i2creceive();
void spiconfig();
unsigned char *PRxData;                   // Pointer to RX data
unsigned char RXByteCtr;
unsigned int RxData;
unsigned char RxBuffer[18];       // Allocate 2 byte of RAM
unsigned char *PTxData;                   // Pointer to TX data
unsigned char TXByteCtr;
char j = 1;
int k;
unsigned int ADC, ADCtest;
//unsigned char tst[5];
const unsigned char TxData[] =            // Table of data to transmit
{
  0x01,
  0x42,
  0x83,
};
const unsigned char TxData2[] =           // Table of data to transmit
{
  0x00
};

void main (void)
{

  addr_t lAddr;
```

```
WDTCTL = WDTPW + WDTHOLD;              // Stop WDT

{
// delay loop to ensure proper startup before SimpliciTI increases DCO
// This is typically tailored to the power supply used, and in this case
// is overkill for safety due to wide distribution.
  volatile int i;
  for(i = 0; i < 0xFFFF; i++){}
}
if( CALBC1_8MHZ == 0xFF )              // Do not run if cal values are erased
{
  volatile int i;
  P1DIR |= 0x03;
  BSP_TURN_ON_LED1();
  BSP_TURN_OFF_LED2();
  while(1)
  {
    for(i = 0; i < 0x5FFF; i++){}
    BSP_TOGGLE_LED2();
    BSP_TOGGLE_LED1();
  }
}

// SimpliciTI will change port pin settings as well
P1DIR = 0xFF;
P1OUT = 0x00;
P2DIR = 0x27;
P2OUT = 0x00;
P3DIR = 0xC0;
P3OUT = 0x00;
P4DIR = 0xFF;
P4OUT = 0x28;

BSP_Init();

if( Flash_Addr[0] == 0xFF &&
    Flash_Addr[1] == 0xFF &&
    Flash_Addr[2] == 0xFF &&
    Flash_Addr[3] == 0xFF )
{
  createRandomAddress();               // set Random device address at initial startup
}
lAddr.addr[0]=Flash_Addr[0];
lAddr.addr[1]=Flash_Addr[1];
lAddr.addr[2]=Flash_Addr[2];
lAddr.addr[3]=Flash_Addr[3];
SMPL_Ioctl(IOCTL_OBJ_ADDR, IOCTL_ACT_SET, &lAddr);
```

```
  BCSCTL1 = CALBC1_8MHZ;                // Set DCO after random function
  DCOCTL = CALDCO_8MHZ;

  BCSCTL3 |= LFXT1S_2;                  // LFXT1 = VLO
  TACCTL0 = CCIE;                       // TACCR0 interrupt enabled
  TACCR0 = 6000;                        // ~ 1 sec
  TACTL = TASSEL_1 + MC_1;              // ACLK, upmode

  // keep trying to join until successful. toggle LEDS to indicate that
  // joining has not occurred. LED3 is red but labeled LED 4 on the EXP
  // board silkscreen. LED1 is green.
  while (SMPL_NO_JOIN == SMPL_Init((uint8_t (*)(linkID_t))0))
  {
    BSP_TOGGLE_LED1();
    BSP_TOGGLE_LED2();;
    __bis_SR_register(LPM3_bits + GIE);     // LPM3 with interrupts enabled
  }
  // unconditional link to AP which is listening due to successful join.
  linkTo();
}

void createRandomAddress()
{
  unsigned int rand, rand2;
  do
  {
    rand = TI_getRandomIntegerFromVLO();    // first byte can not be 0x00 of 0xFF
  }
  while( (rand & 0xFF00)==0xFF00 || (rand & 0xFF00)==0x0000 );
  rand2 = TI_getRandomIntegerFromVLO();

  BCSCTL1 = CALBC1_1MHZ;                // Set DCO to 1MHz
  DCOCTL = CALDCO_1MHZ;
  FCTL2 = FWKEY + FSSEL0 + FN1;         // MCLK/3 for Flash Timing Generator
  FCTL3 = FWKEY + LOCKA;                // Clear LOCK & LOCKA bits
  FCTL1 = FWKEY + WRT;                  // Set WRT bit for write operation

  Flash_Addr[0]=(rand>>8) & 0xFF;
  Flash_Addr[1]=rand & 0xFF;
  Flash_Addr[2]=(rand2>>8) & 0xFF;
  Flash_Addr[3]=rand2 & 0xFF;

  FCTL1 = FWKEY;                        // Clear WRT bit
  FCTL3 = FWKEY + LOCKA + LOCK;         // Set LOCK & LOCKA bit
}

//////////////////////////////////////////////////////////////////////////////////
```

```
////////////////////////////////////////////////////////////////////////////////

void Setup_TX(void){
  _DINT();
  IE2 &= ~UCB0RXIE;
  while (UCB0CTL1 & UCTXSTP);             // Ensure stop condition got sent// Disable RX interrupt
  UCB0CTL1 |= UCSWRST;                    // Enable SW reset
  UCB0CTL0 = UCMST + UCMODE_3 + UCSYNC;    // I2C Master, synchronous mode
  UCB0CTL1 = UCSSEL_2 + UCSWRST;           // Use SMCLK, keep SW reset
  UCB0BR0 = 12;                           // fSCL = SMCLK/12 = ~100kHz
  UCB0BR1 = 0;
  UCB0I2CSA = 0x48;                       // Slave Address is 048h
  UCB0CTL1 &= ~UCSWRST;                   // Clear SW reset, resume operation
  IE2 |= UCB0TXIE;                        // Enable TX interrupt
}
void Transmit(void){
    PTxData = &MSData;                    // TX array start address
    TXByteCtr = NUM_BYTES_TX;             // Load TX byte counter
    while (UCB0CTL1 & UCTXSTP);           // Ensure stop condition got sent
    UCB0CTL1 |= UCTR + UCTXSTT;           // I2C TX, start condition
    __bis_SR_register(CPUOFF + GIE);      // Enter LPM0 w/ interrupts
}

void Receive(void)
{
  IE2 &= ~UCB0TXIE;
  P3SEL = 0x00;
  volatile unsigned int i;
  volatile unsigned int k;
  int address2[] = {1,1,0,0,0,0,1,1,0,0,0,0,0,0,1,1,0,0,0};  // Address is 0x91
  WDTCTL = WDTPW + WDTHOLD;               // Stop watchdog timer
  P3DIR |= 0x3F;                          // Set P4.5 to output direction
  P3OUT = 0x06;
  P3OUT &= ~0x02;
  ///////////////////////Address////////////////
  for(k=0; k<=18; k++){
    for(i=0; i<=1; i++);
      P3OUT ^= 0x04;                      // Toggle P4.5 using exclusive-OR
      if(address2[k])
        P3OUT |= 0x02;
      else
        P3OUT &= ~0x02;
  }
  P3OUT &= ~0x02;
  for(i=0; i<=1; i++);
```

```
  P3DIR = 0x3D;                        // Set P4.5 to output direction
  ///////////////////////Receive1////////////////
  for(k=0; k<=8; k++){
    P3OUT ^= 0x04;                     // Toggle P4.5 using exclusive-OR
    if(0x42 & P3IN)
      RxBuffer[k] = 1;
    else
      RxBuffer[k] = 0;
    for(i=0; i<=1; i++);
    P3OUT ^= 0x04;
    for(i=0; i<=1; i++);
  }
  ///////////////////////Receive2////////////////
  for(k=8; k<=16; k++){
    P3OUT ^= 0x04;                     // Toggle P4.5 using exclusive-OR
    if(0x42 & P3IN)
      RxBuffer[k] = 1;
    else
      RxBuffer[k] = 0;
    for(i=0; i<=1; i++);
    P3OUT ^= 0x04;
    for(i=0; i<=1; i++);
  }
  P3DIR = 0xCF;
  P3OUT = 0x06;
  for(i=0; i<25; i++);      // Stop condition
}

void linkTo()
{
  linkID_t linkID1;
  uint8_t  msg[5];
  int i;

  // keep trying to link...
  while (SMPL_SUCCESS != SMPL_Link(&linkID1))
  {
    __bis_SR_register(LPM3_bits + GIE);     // LPM3 with interrupts enabled
    BSP_TOGGLE_LED1();
    BSP_TOGGLE_LED2();
  }


  // Turn off all LEDs
  if (BSP_LED1_IS_ON())
  {
    BSP_TOGGLE_LED1();
```

```
}
if (BSP_LED2_IS_ON())
{
  BSP_TOGGLE_LED2();
}
//UCB0CTL0 = 0x00;
BSP_TURN_ON_LED1();

WDTCTL = WDTPW + WDTHOLD;              // Stop WDT

FLL_CTL0 |= XCAP14PF;                  // Configure load caps
for (i = 0; i < 10000; i++);           // Delay for 32 kHz crystal to
                                       // stabilize

SD16CTL = SD16SSEL0;          // 1.2V ref, SMCLK
SD16CTL |= SD16REFON;
SD16CCTL0 |= SD16SNGL + SD16UNI;        // Single conv Unipolar
for (i = 0; i < 0x3600; i++);           // Delay for 1.2V ref startup

// I2C configuration transmit process
P3SEL |= 0x06;                         // Assign I2C pins to USCI_B0
Setup_TX();
RPT_Flag = 1;
MSData = 0x01;
Transmit();
while (UCB0CTL1 & UCTXSTP);            // Ensure stop condition got sent
MSData = 0x42;
Transmit();
while (UCB0CTL1 & UCTXSTP);            // Ensure stop condition got sent
MSData = 0x83;
Transmit();
while (UCB0CTL1 & UCTXSTP);            // Ensure stop condition got sent
MSData = 0x00;
Transmit();
while (UCB0CTL1 & UCTXSTP);            // Ensure stop condition got sent
P3SEL = 0x00;
P3DIR = 0xCF;
P3OUT = 0x06;
for(i=0; i<25; i++);     // Stop condition
SD16CTL |= SD16REFON;                                          // Internal 1.2V ref on
DAC12_0CTL = DAC12IR + DAC12SREF_3 + DAC12AMP_5 +        // SD16 Ref,
                                DAC12OPS + DAC12ENC + DAC12CALON;
DAC12_0DAT = 0x000;                                            // 2.58V

while (1)
{
```

```
  if(DAC12_0DAT < 0xAAA)
    DAC12_0DAT = DAC12_0DAT + 0x0F0;
  else
    DAC12_0DAT = 0x000;
//ADC Conversion
  SD16CTL |= SD16REFON;
  SD16CCTL0 |= SD16SC;                  // Set bit to start conversion
  while ((SD16CCTL0 & SD16IFG)==0);      // Poll interrupt flag
  results = SD16MEM0;                   // Save CH0 results (clears IFG)
  ADC = results*(1.2/2)/65536;

//Receive process
  Receive();
  RxData = 0x000;
  for(i=0; i<12; i++){
    RxData += RxBuffer[i];
    RxData = RxData << 0x01;
  }



__no_operation();                       // Set breakpoint >>here<< and
                                  // read out the RxBuffer buffer
  SMPL_Ioctl( IOCTL_OBJ_RADIO, IOCTL_ACT_RADIO_SLEEP, "" );
  __bis_SR_register(LPM3_bits+GIE);      // LPM3 with interrupts enabled
  SMPL_Ioctl( IOCTL_OBJ_RADIO, IOCTL_ACT_RADIO_AWAKE, "" );

  BSP_TOGGLE_LED2();

  //msg[0] = 42;
  //msg[1] = 5;
  //msg[0] = 0x4E;
  //msg[0] = ADC;
  ADCtest = 0x4EF;
  ADC = ADCtest*2;
  msg[0] = ((RxData/1000)%10);
  msg[1] = ((RxData/100)%10);
  msg[2] = ((RxData/10)%10);
  msg[3] = ((RxData/1)%10);
  msg[4] = RxBuffer[0];

  if (SMPL_SUCCESS == SMPL_Send(linkID1, msg, sizeof(msg)))
  {
    BSP_TOGGLE_LED2();
  }
  else
  {
```

```
    BSP_TOGGLE_LED2();
    BSP_TOGGLE_LED1();
   }
  }
}



/*-----------------------------------------------------------------------------
* ADC10 interrupt service routine
-----------------------------------------------------------------------------
#pragma vector=ADC10_VECTOR
__interrupt void ADC10_ISR(void)
{
  __bic_SR_register_on_exit(CPUOFF);        // Clear CPUOFF bit from 0(SR)
}
*/
/*-----------------------------------------------------------------------------
* Timer A0 interrupt service routine
-----------------------------------------------------------------------------*/
#pragma vector=TIMERA0_VECTOR
__interrupt void Timer_A (void)
{
  __bic_SR_register_on_exit(LPM3_bits);        // Clear LPM3 bit from 0(SR)
}

//-----------------------------------------------------------------------------
// The USCI_B0 data ISR is used to move received data from the I2C slave
// to the MSP430 memory. It is structured such that it can be used to receive
// any 2+ number of bytes by pre-loading RXByteCtr with the byte count.
//-----------------------------------------------------------------------------
#pragma vector = USCIAB0TX_VECTOR
__interrupt void USCIAB0TX_ISR(void)
{
    if (TXByteCtr)                    // Check TX byte counter
  {
   UCB0TXBUF = MSData;                // Load TX buffer
   TXByteCtr--;                       // Decrement TX byte counter
  }
  else
  {
   if(RPT_Flag == 1){
   RPT_Flag = 0;
   PTxData = &MSData;                 // TX array start address
   TXByteCtr = NUM_BYTES_TX;          // Load TX byte counter
   __bic_SR_register_on_exit(CPUOFF);
   }
```

```
    else{
    UCB0CTL1 |= UCTXSTP;                    // I2C stop condition
    IFG2 &= ~UCB0TXIFG;                     // Clear USCI_B0 TX int flag
    __bic_SR_register_on_exit(CPUOFF);      // Exit LPM0
    }
  }
}
```